Post-interventional vascular remodeling: novel insights and therapeutic strategies

Sluiter, T.J.

CHAPTER 9

Blockade of YAP mechano-activation prevents neointima formation and adverse remodeling in arterialized vein grafts

Gloria Garoffolo[1], Thijs J. Sluiter[2], Anita Thomas[3], Luca Piacentini[1], Matthijs S. Ruiter[1], Alessia Schiavo[1], Massimo Salvi[4], Claudio Saccu[1], Stefano Zoli[1], Mattia Chiesa[1], Takumi Yokoyama[2], Marco Agrifoglio[1], Monica Soncini[5], Gianfranco B. Fiore[5], Fabio Martelli[6], Gianluigi Condorelli[7,8], Paolo Madeddu[3], Filippo Molinari[4], Umberto Morbiducci[4], Paul H.A. Quax[2], Gaia Spinetti[9], Margreet R. de Vries[2,10] and Maurizio Pesce[1,4,11,*]

[1]Centro Cardiologico Monzino, IRCCS. Milan, Italy
[2]Einthoven Laboratory for Experimental Vascular Medicine, Department of Surgery; Leiden University Medical Center (LUMC). Leiden, the Netherlands
[3]Bristol Medical School; University of Bristol. Bristol, United Kingdom
[4]Dipartimento di Ingegneria Meccanica e Aerospaziale; Politecnico di Torino. Turin, Italy
[5]Dipartimento di Bioingegneria, Elettronica ed Informazione; Politecnico di Milano. Milan, Italy
[6]Laboratorio di Cardiologica Molecolare; IRCCS Policlinico San Donato. Milan, Italy
[7]Humanitas Cardio-Center; IRCCS Humanitas Research Hospital. Rozzano, Italy
[8]Department of Biomedical Sciences; Humanitas University. Pieve Emanuele, Italy
[9]Unità di Ricerca Cardiovascolare; IRCCS Multimedica. Milan, Italy
[10]Department of Surgery; Brigham & Women's Hospital and Harvard Medical School. Boston, MA, USA
[11]Department of Cell Biology; King Faisal Specialist Hospital & Research Center. Riyadh, Saudi Arabia

Journal of American Heart Association 2025 April 1 14(7):037531

ABSTRACT

Background: Bypass surgery using saphenous vein (SV) grafts is commonly used to revascularize ischemic heart and lower limbs. These interventions have limited success due to adverse remodeling caused by over-proliferation of smooth muscle cells in the intima layer leading to progressive bypass stenosis. We previously showed that cyclic strain deriving from exposure to coronary flow induces the expression of the matricellular protein Thrombospondin-1 (TSP-1) in the human SV, promoting activation of progenitor cells normally residing in the adventitia.

Methods: We analyzed the data of an RNA-sequencing profiling of human saphenous vein progenitors (SVPs) subjected to uniaxial strain previously performed by us. Experiments in cell culture, ex vivo and in vivo vein arterialization models were performed to substantiate findings with particular reference to the role of mechanically activated transcription factors. Validation was performed in vitro and in ex vivo/in vivo models of vein graft disease (VGD).

Results: Bioinformatic assessment of the RNA-sequencing data indicated Yes associated protein (YAP) as a possible mechanically-regulated effector in pathologic evolution of SVPs. Inhibition of YAP by Verteprofin (VTP) - a drug that abolishes the interaction of YAP with Tea Domain DNA (TEAD) binding proteins - reduced the expression of pathologic markers in vitro, and in vivo, reduced intima hyperplasia.

Conclusions: Our results reveal that desensitizing the SV-resident cells to mechano activation of YAP is feasible to reduce the graft disease progression.

CLINICAL PERSPECTIVE

What is new?

• With this contribution, we show the involvement of the YAP mechanically-activated pathway in the pathological remodeling of the venous coronary artery bypasses.

What are the clinical implications?

• We show the feasibility of a 'mechano-therapeutic' approach to reduce the impact of vein graft disease, by pharmacologically targeting molecular pathways involved in cellular mechanosensation.

INTRODUCTION

Despite the high performance of percutaneous coronary interventions (PCI) and the superiority of arterial conduits - e.g., the inner mammary artery (IMA) or the radial artery (RA) - in maintaining graft patency at mid/long-term[1], the use of venous bypass conduits is still very common in coronary surgery[2], especially in multi-vessel coronary artery disease (CAD)[3]. Vein grafts are also frequently used in surgical treatment of peripheral artery disease, where SV implantation is still superior to endovascular treatment[4]. While the choice of the SV is justified by easiness of harvesting, length, manufacturability and an excellent mechanical resistance, it has also severe limitations deriving from a maladaptive remodeling process that initiates shortly after implantation. This triggers progressive occlusion and formation of atherosclerotic plaques in a high percentage of patients. This process, known as vein graft disease (VGD), has various pathophysiological causes, including mechanical damages to the endothelium and/or the vessel wall due to physical manipulation during harvest, exposure to the high arterial pressure/flow regimen, hypoxia, intraplaque angiogenesis, inflammation, lipid accumulation and secondary atherosclerosis[5-7].

At a cell biology level, VGD is caused by over-proliferation of cells with smooth muscle cell (SMC)-like characteristics in the vein wall. These cells may originate from pre-existing SMCs that undergo a phenotypic switch from contractile to secretory and/or from progenitors residing in the adventitia[8-10], which migrate towards the sub-endothelial (intima) layer and accumulate to reduce the patency of the graft by an 'inward' growing process[5]. Extensive research highlighted several molecular effectors potentially involved in SV maladaptive remodeling. These include innate immunity effectors, chemokines, or matrix-remodeling enzymes[7]. The success of targeting these factors to reduce VGD in patients has been, unfortunately, limited[6,11,12]. In an effort to delineate novel pathophysiological mechanisms in VGD, we have pursued a bioengineering program to assess the role of mechanical forces in the failure of the SV coronary artery bypass grafts (CABG). We have previously found that exposure of human SVs to pulsatile coronary-like flow[13] generates a matricellular signaling mediated by TGF-β1 and TSP-1, which recruits resident progenitors with SMC-like characteristics to initiate the process of vascular remodeling[14].

In the present study, we employed RNA sequencing to identify mechanically-activated transcriptional pathways connected to direct myofibroblast differentiation of these progenitors[15,16]. We identified numerous genes that are modulated by mechanical stimulation, including those participating in the transcriptional network dependent on YAP, a key transcription factor, belonging to the Hippo pathway[17,18]. Cell biology experiments confirmed the involvement of YAP in the acquisition of a myofibroblast phenotype[19]. To reduce mechanical activation of adventitial progenitors, we utilized VTP, an inhibitor of the transcriptional complex formed by YAP and the transcriptional co-activator with PDZ-binding motif (TAZ) complex, which we recently found to inhibit fibrosis in the ischemic heart[20] and to reduce pathologic

activation of human valve interstitial cells[21]. SVPs treated with the drug exhibited reduced migratory ability and a reduced formation of focal adhesion contacts[22]. VTP also reduced interaction of YAP with pSMAD3, a transcriptional activator downstream of TGF-β1, blunted the expression of αSMA, TSP-1 and fibronectin (FN), and significantly inhibited expression/secretion of collagen. VTP, finally, substantially reduced the extent of fibrosis and adverse remodeling in a mouse model of vein graft failure[23].

MATERIALS AND METHODS

A complete methodological section is available in **Data S1**. Lists of the primers sequences and the antibodies used in the study are provides in **Table S1** and **Table S2**, respectively. The data that support the findings of this study are available from the corresponding author upon reasonable request.

Ethical statement of in vivo procedures

The use of human SV material (recovered during saphenectomy or harvesting for CABG, patient characteristics in **Table S3**) for ex vivo experiments and cell culture has been authorized by the Ethical Committee at Centro Cardiologico Monzino, IRCCS. Patients were required to sign an informed consent. The use of human material was performed in compliance with the Declaration of Helsinki. For the in vivo SV arterialization model in pigs[24], animals received humane care in accordance with the Home Office Animals (Scientific Procedures) Act of 1986 and the Guide for the Care and Use of Laboratory Animals published by the US National Institutes of Health (NIH Publication No. 85- 23, revised 1996). The trial of vena cava into carotid artery transplantation in mice was performed according an experimental procedure authorized by the institutional committee of the Leiden University Medical Center approved all animal experiments licensed under project number (AVD1160020172409). These animal experiments were performed in compliance with Dutch government guidelines and the Directive 2010/63/EU of the European Parliament.

Statistical analyses

The statistics analyses supporting the bioinformatics analysis of the RNAseq data are reported in the specific section of the extended online methods. The type of statistical tests to compare data presented in the bar graphs throughout the study are specified in figure legends. Each bar has superimposed the number of experimental replicates (performed on independent mice and cell lines), and a $P < 0.05$ was considered a significant value in statistical comparisons. Data were analyzed and graphically represented using the GraphPad software. In every graph, data are represented as mean ± SEM. Before performing statistical analyses, normality and outliers' tests were performed. The type of statistical test used to compare data is specified in the legend of each figure. For single comparisons we used two-tail paired or unpaired t-test. For multiple comparisons we used one-way ANOVA with Tukey or Dunnet post-hoc. Differential gene expression in RNAseq analysis were corrected by the Benjamini Hochberg method, considering differentially expressed genes with an adjusted P – value < 0.05. Please refer to the legend of figures and supplementary material for further details.

RESULTS

Cyclic strain-dependent gene regulation in human SVPs increases YAP transcriptional signaling

We assessed the general effects of uniaxial straining on the global transcriptome of human adventitial progenitors[15,16]. The condition of mechanically stimulated vs. statically cultured SVPs ("ON" vs. "OFF" comparisons) determined reorientation of the cells along a preferentially orthogonal direction to the strain field and changes in cellular form factors (**Figure 1A**). RNA-sequencing performed using total RNA from mechanically stimulated (ON) vs statically cultured (OFF) cells for 72 hours highlighted several hundred modulated genes (**Figure 1B**)[25]. In order to derive a signature of the mechanically regulated genes, we performed a differential gene expression analysis. This resulted in a list of 155 upregulated and 259 downregulated genes ($|log2FC|>1$ and adjusted P-Value <0.05; **Dataset S1**) in the mechanically stimulated vs. static cultured cells (ON vs. OFF condition). Gene ontology enrichment analysis showed the existence of mechanically-regulated pathways (**Figure 1C**), including genes related to extracellular matrix organization, cell adhesion to matrix components, proliferation and response to fibrotic signaling (**Dataset S2-S3**). In other cell types (e.g. cardiac fibroblasts) uniaxial strain dose-dependently increases nuclear translocation of the transcription factor YAP[26]. We therefore directed our bioinformatic survey to assess changes in regulation the Hippo signaling components, and putative YAP transcriptional targets (**Figure 1D** and **S1A**). This revealed a consistent modulation of genes with a functional annotation as YAP targets and components of the Hippo pathway, according to GO and KEGG terms. Validation of results by RT-qPCR (**Figure 1D**) confirmed the effect of mechanical strain on expression of key members of the TGF-β pathway suggesting, as already reported[27], a functional convergence involving YAP as a common determinant. RT-qPCR did not confirm (with the exception of FZD8) relevance of genes belonging to the Wnt-activated signaling, as possible YAP targets affected by mechanical stimulation (**Figure S1B**).

To further confirm the importance of YAP in strain-dependent SVPs activation, we assessed whether the morphological changes determined by the mechanic stimulation (**Figure 1A**), also induced nuclear translocation of the transcription factor. A clear increase in nuclear YAP was observed upon mechanical activation of SVPs, indicative of YAP transcriptional activation (**Figure 1E**). Furthermore, mechanical stimulation decreased phosphorylation of YAP (pYAP) at Ser^{127}, which normally promotes cytoplasmic retention[28]. The nuclear translocation of YAP was not associated, however, with an imbalance in expression and phosphorylation levels of LATS, a component of the hippo pathway upstream of YAP[17,29,30] (**Figure 1F**). Consistently with the increased nuclear translocation, expression of canonical YAP target genes CTGF, CYR61 and ANKRD120,21 as well as the physical interaction with TEAD1-4 DNA binding proteins[31] was significantly increased in mechanically stimulated cells (**Figure 1G, H**), as demonstrated by RT-qPCR and by the increased

intensity of the TEAD1-4 band in immunoprecipitation/western blot analyses (see also quantification of the TEAD1-4/YAP ratio, revealed by densitometric analysis).

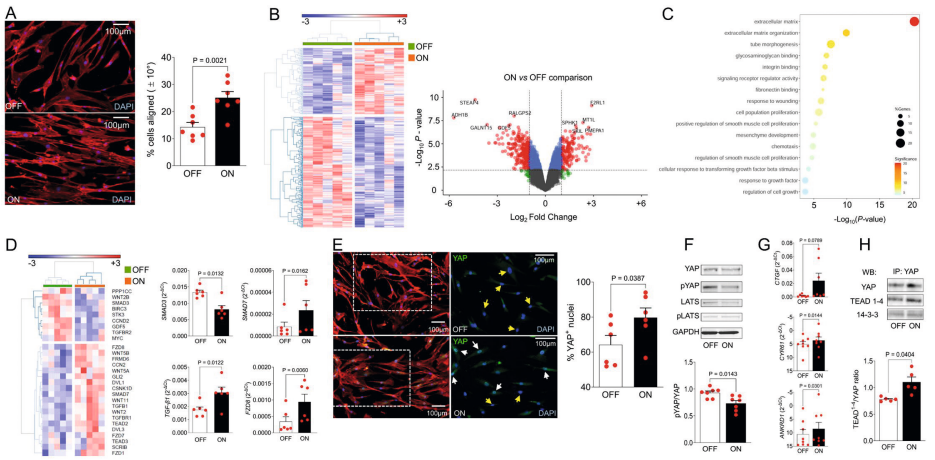

Figure 1. Mechano-sensitivity of human SVPs and activation of YAP-dependent signaling.

(**A**) Human SVPs subjected to cyclic strain (10% elongation, 1 Hz frequency) for 72 underwent extensive orientation changes. Cell were stained with phalloidin TRITC (red) and DAPI. The graph indicates the difference in the alignment of the major axis of the nuclei (indicative of orientation of the whole cellular body) in a perpendicular direction to the direction of the strain (vertical in the lower micrograph). (**B**) Heatmap representing the results of an unsupervised cluster analysis and relative volcano plot indicating the genes that, by RNAseq, were found to be differentially expressed in mechanically stimulated (ON) *vs.* statically cultured (OFF) SVPs for 72 hours. Red dots in volcano plot represent genes that are up-/dow-modulated by$|\log_2 FC|>1$ and an adjusted $P<0.05$. (**C**) Bubble plot representing upregulated Gene Ontology (GO) pathways significantly enriched in the ON *vs.* OFF comparison. As it is evident, this comparison produced enrichment of numerous pathways connected with extracellular matrix remodeling and binding, smooth muscle cells proliferation and differentiation. (**D**) Unsupervised cluster analysis of the differentially expressed genes with a Hippo pathway functional annotation. The heatmap shows a majority of genes that were upregulated in the ON vs. OFF condition. This included genes belonging to the TGF-β pathways (e.g. TGFBR1, TGFB1, SMAD7) and Wnt-dependent signaling (e.g. FZD1/8, WNT5A, GLI2, DVL1/3). Part of these genes were confirmed by RT qPCR on independent RNA samples (see graphs on the right of the panel with indication of the significance in pairwise comparison). (**E**) Effect of cyclic straining on YAP nuclear translocation. An immunofluorescence staining of cells cultured in static or dynamic conditions for 72 hrs was performed with YAP-specific antibodies, followed by quantitative analysis of nYAP+ and nYAP- cells (white and yellow arrows, respectively). Pairwise comparison of the two conditions revealed a significant increase of nYAP+ cells in dynamically cultured cells. (**F**) Mechanical stimulation led to a significant decrease of YAP phosphorylation at Ser. This was independent of the Hippo kinase pathway modulation, as demonstrated by an equal level of pLATS. (**G**) Assessment of canonical YAP transcriptional targets CTGF, ANKRD1 and CTGF expression under static and dynamic conditions establishes the role of YAP as a transcriptional mechanosensory in SVPs. (**H**) TEAD1-4, but not 14-3-3 interaction with YAP is increased in mechanically-stimulated cells, as shown by immunoprecipitation/ western analysis followed by quantification. In all graphs, red dots overlapped to the bars indicate the result of each experiment performed in independent cell lines. The data represented in the bar graph in panels A, D, F, G and H were compared by pairwise t-test. The P values are indicated above the significance lines.

YAP function in human SVP is stress fibers-dependent

Cytoskeleton tensioning due to transmission of mechanical forces or adhesion on geometrically patterned adhesive substrates is connected to cytoskeleton-dependent activation of YAP transcriptional signaling with variation in cell responses such as migration and proliferation[17,29]. We previously showed that adhesion of fibroblast-like cells onto substrates (plastic or glass) with a Young's elastic modulus in the range of Mega Pascal (MPa) is, per se, a mechanically sufficient stimulus to observe robust YAP nuclear signaling caused by firm adhesion and stress fibers polymerization20. Since in previous studies inhibition of F actin by protein Kinase A (PKA) reduced YAP/TEAD dependent smooth muscle cells proliferation[32], we tested the effects of Forskolin (FRSK), a pharmacological stimulator of cAMP production and PKA activation with direct effects on actin cytoskeleton[33]. Treatment with FRSK resulted in partial depolymerization of the F-actin cytoskeleton of SVPs and this was associated to a reduction in the percentage of cells that exhibited a clear nuclear localization of YAP (**Figure 2A**, top right). In order to assess how the pharmacological treatment interferes with YAP localization, we quantified YAP fluorescence using Image-J or a proprietary algorithm (CARE) that was devised specifically for automated segmentation of fluorescence images[34]. This enabled us to determine the nuclear/cytoplasm YAP expression ratio. As shown in **Figure 2A**, bottom, addition of FRSK in the medium caused a significant relocation of the YAP fluorescence from the nucleus to the cytoplasm, while removal of the drug restored YAP nuclear localization. In keeping with previous results showing that YAP nuclear localization is regulated by direct phosphorylation[35], western analysis confirmed an elevation of phospho-YAP in cells treated with FRSK (**Figure 2B**, left). Negative transcriptional regulation of CTGF, and at a more extent of CYR61 and ANKRD1, direct YAP transcriptional targets, followed the trend of YAP nuclear shuttling in cells treated with FRSK (**Figure 2B,** right). Finally, to assess whether mechanical stimulation was also related to an increase in cellular motility (another cellular mechanism regulated by YAP[36]), we performed migration tests with SVPs exposed to cyclic strain (or not) and in the presence or the absence of PKA activator. This showed that mechanically stimulated SVPs had a higher migratory ability, and this migration was inhibited by depolymerization of the cytoskeleton (**Figure 2C**). A more direct role of YAP and TEAD in migratory activity of SVPs was finally assessed by genetically interfering with YAP expression by treating cells with specific siRNAs. As shown in **Figure 2D**, the use of YAP and TEAD specific siRNAs abolished the SVPs migration, thus confirming a direct role of the YAP transcriptional function in SVPs motility.

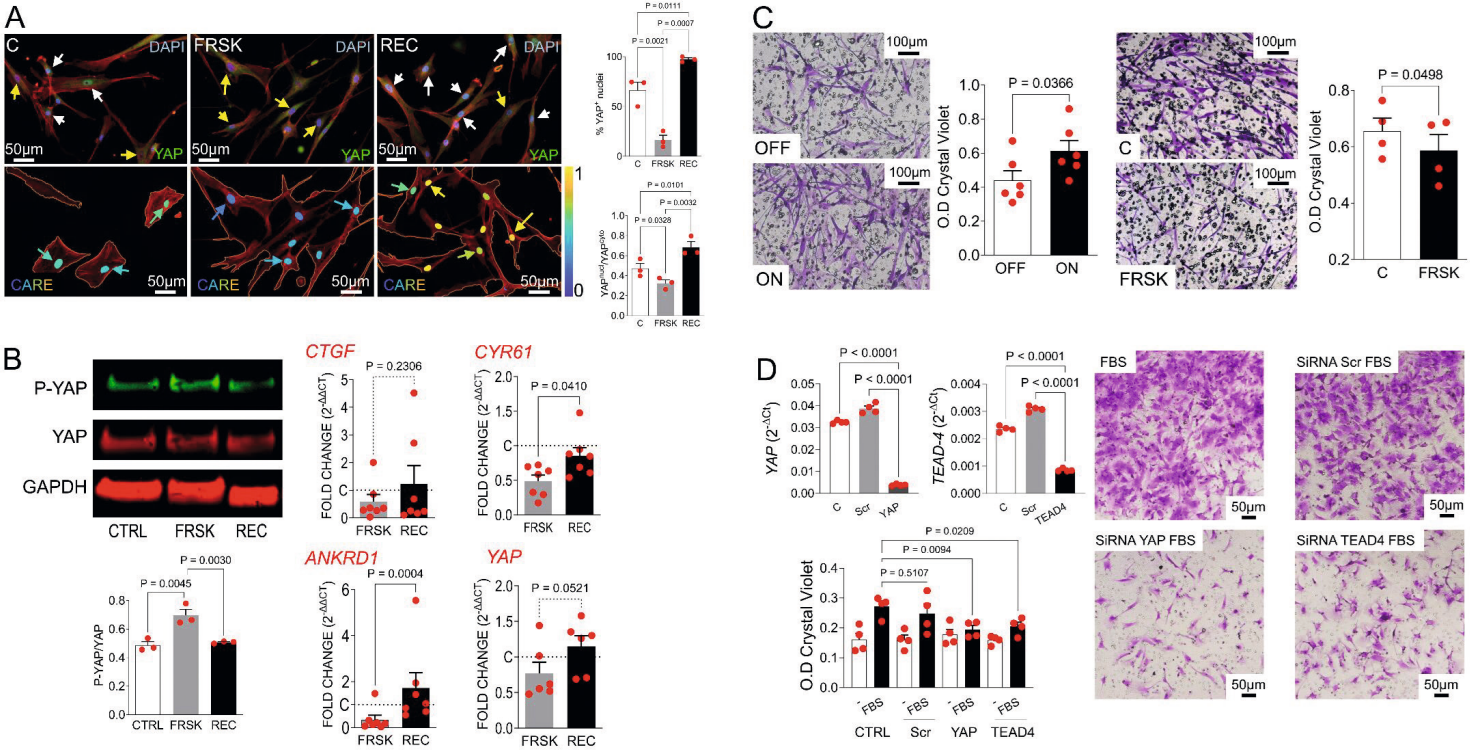

Figure 2. Dependency of YAP transcriptional activation by cytoskeleton tensioning.

(A) SVPs plated into dishes with MPa mechanical compliance were treated with Forskolin, an activator of the Adenylate Cyclase and the cAMP/PKA pathway, for 6 hours followed by recovery for an overnight period. The panels on top show the reversible depolymerization of the F-Actin cytoskeleton. White arrows indicate cells with $nYAP^{+}$ nuclei, while white arrows show $nYAP^{-}$ cells; quantification of these cells is shown in the upper right bar graph. The images on the bottom of the panel show the rendering of the YAP^{nucl}/YAP^{cyto} ratio as detected by CARE algorithm. The nuclei of the cells (and the arrows pointing at some of these nuclei) are represented with a different color to discriminate differences in the YAP^{nucl}/YAP^{cyto} ratio. The color code adopted for this representation is indicated in the bar on the right side of the panels and graphic representation of the YAP^{nucl}/YAP^{cyto} ratio is included in the lower right bar graph.
(B) Western/RT-qPCR analyses to detect the effects of FRSK treatment on YAP phosphorylation (^{127}Ser) and expression of canonical target genes. As shown in the western analysis, treatment of SVPs with the PKA activator transiently increased the level of YAP phosphorylation, consistent with the reversible effect on nuclear localization observed in panel A. Inhibition of canonical targets *CTGF*, *CYR61* and *ANKRD1* also showed a transient inhibition of the YAP transcriptional activity (more pronounced for *CYR61* and *ANKRD1*) and the downregulation of the YAP gene itself.
(C) Transwell migration assay of static and dynamically-cultured SVPs for 72hrs. As shown in the panels on the left, mechanically-stimulated cells (72hrs) migrated more efficiently than those maintained in static culture. Treatment with FRSK inhibited this effect (panel on the right).
(D) Implication of YAP and TEAD transcription factors in SVPs migration was assessed by siRNA-mediated knockdown experiment. The upper left graphs indicate the downregulation of both transcription factors at a transcriptomic level by RT-qPCR vs. the control and the scrambled siRNAs. The micrographs on the right show an example of a transwell migration assay performed with control, scrambled siRNA and YAP/TEAD4 siRNA sequences. As shown, siRNA-mediated downregulation of both transcription factors reduced SVPs motility. Quantification of the SVPs motility is shown in the bottom bar graph. Data in bar graphs were compared by one-way Anova (repeated measures) with Tukey (panels A, B, D; western blot or RT-qPCR) or Dunnet post-hoc tests (panel D, migration), and by paired t-test in the other graphs. In all graphs, red dots overlapped to the bars indicate the result of each experiment performed in independent cell lines. The P values are indicated above the significance lines.

Cooperation of YAP signaling with TGF-β downstream targets establishes a molecular basis for SMC- like differentiation of SVPs.

Cooperation of YAP signaling with TGF-β downstream targets establishes a molecular basis for SMC-like differentiation of SVPs. We previously showed that profibrotic signaling in arterialized veins might depend on a mechanically-activated pathway involving the TGF-β/TSP-1 axis[14]. Therefore, we interrogated the set of the up-regulated genes in SVPs in the ON vs. OFF conditions, searching for targets containing known binding sequences for transcription factors. By this search we identified gene modules potentially regulated by a number of DNA-binding factors (**Figure 3A, Dataset S4**), among which TEAD4, one of the natural molecular interactors of the YAP/TAZ complex[37,38], was enriched. A gene ontology analysis of the genes potentially regulated by TEAD4 in the same gene set was then performed, and this led to identify numerous pathways related to extracellular matrix remodeling and response to TGF-β signaling (**Figure 3B, Dataset S5**). In order to mechanistically substantiate the convergence of YAP/TAZ and TGF-β pro-fibrotic signaling upon mechanical-dependent activation of SVPs, we plated SVPs onto MPa substrate with or without stimulation with TGF-β,

TSP-1, or combination of the two (T+T condition). We then assessed the YAP nucleus/cytoplasmic ratio and determined expression of PCNA and SM22α. Results showed that the T+T combination yielded the highest level of nuclear YAP translocation (**Figure 3C**), and significantly increased growth and SMC differentiation of SVPs (**Figure 3D**). These findings were corroborated by an increase in phosphorylation of SMAD2 and SMAD3, the most relevant nuclear transducers of TGF-β profibrotic signaling[39], in cells treated with the T+T combination (**Figure S2**).

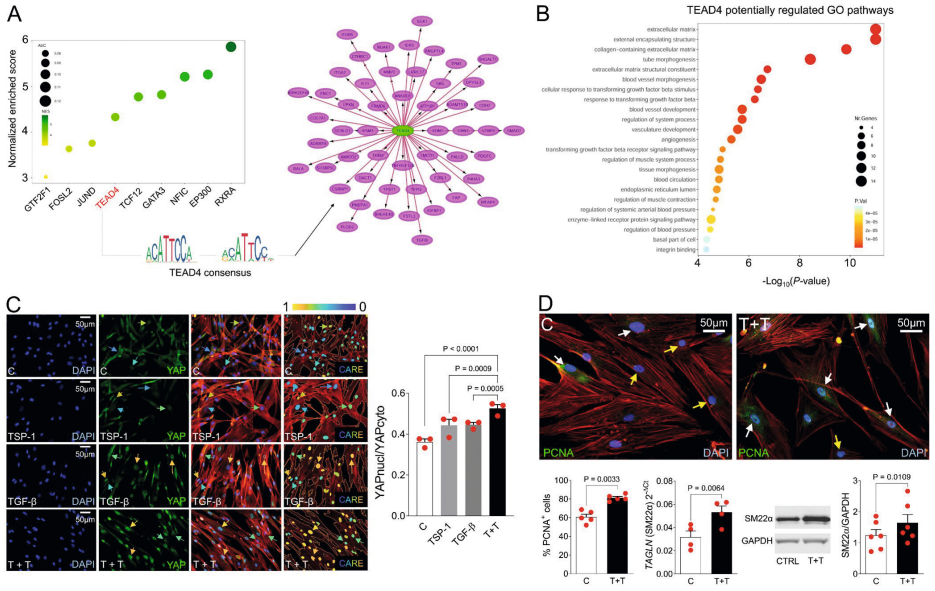

Figure 3. Cooperation of TEAD4/TGF-β transcriptional signaling to mechano-activation of human SVPs.

(**A**) Bubble plot representing the most represented group of genes containing in their promoter consensus binding sequences of the indicated transcription factors. TEAD4, indicated in red, is one of the most common YAP transcriptional interactors in transcriptional complexes. The gene network represented on the right of the panel indicates the genes that contain the TEAD4 consensus in their promoters and are putatively regulated by YAP/TEAD4 complexes. Note the presence of numerous genes linked to extracellular matrix binding and remodeling, YAP target genes and genes connected to TGF-β signaling.
(**B**) Bubble plot representation of an enrichment analysis of the genes containing the two TEAD4 consensus biding sequences represented in **panel A**. Among these pathways, again, there was an association of genes to extracellular matrix remodeling and binding and response to TGF-β, suggesting a functional cooperation of the YAP/TEAD4 complex with the TGF-β signaling.
(**C**) Potentiation of the YAP-dependent signaling by TGF-β and TSP-1. The panels show an immunofluorescence staining of SVPs plated onto MPa substrates in the presence of TGF-β, TSP-1, or a combination thereof (T+T). As shown in the IF panels addition of the single factors enhanced YAP nuclear translocation compared to controls. The T+T combination was, however, the most effective as evidenced by the analysis of the YAP nuclear/cytoplasmic ratio with CARE, an algorithm that we previously developed to perform automatic segmentation and fluorescence quantification of immunofluorescence images[34].

(**D**) Stimulation with T+T increased the proliferation of SVPs and the expression (both at RNA and protein levels) of SM22α early SMC marker. On the top of the panel it is represented an immunofluorescence of PCNA as a cell growth marker, while of the bottom there is the quantification of PCNA together with the quantification of *TAGLN* (SM22α) RNA by RT-qPCR and protein by western analysis.
Statistical comparisons were performed by one-way Anova (repeated measures) with Tukey post-hoc in panel **C** and by paired t-test in panel **D**. In all graphs, red dots overlapped to the bars indicate the result of each experiment performed in independent cell lines. The *P* values of pairwise t-test are indicated above the significance lines.

Implication of YAP signaling in vein arterialization process.

We next investigated the direct involvement of YAP in the vein arterialization process. To this aim, we assessed the expression of the transcription factor using, ***i)*** human SVs exposed to either venous flow or coronary flow/pressure[13,14], ***ii)*** a porcine *in vivo* vein graft model (SV interposition in carotid)[39] and, ***iii)*** a time course of murine *in vivo* vein graft model, (caval vein interposition in carotid)[23]. The results of immunohistochemistry staining with YAP specific antibodies exhibited, especially in the porcine and mouse models, a progressive increase in the number of cells with nuclear YAP (nYAP^{+} cells) (**Figure 4**). It was interesting to note that cells with nuclei with a more elongated shape and apparently aligned in the direction of the circumferential component of the hemodynamic force in the graft wall[14], resulted to contain higher amount of nuclear YAP. This extends our previous observations showing the effects of compression forces on nuclear YAP translocation in cardiac fibroblasts in post-ischemic myocardial remodeling[20].

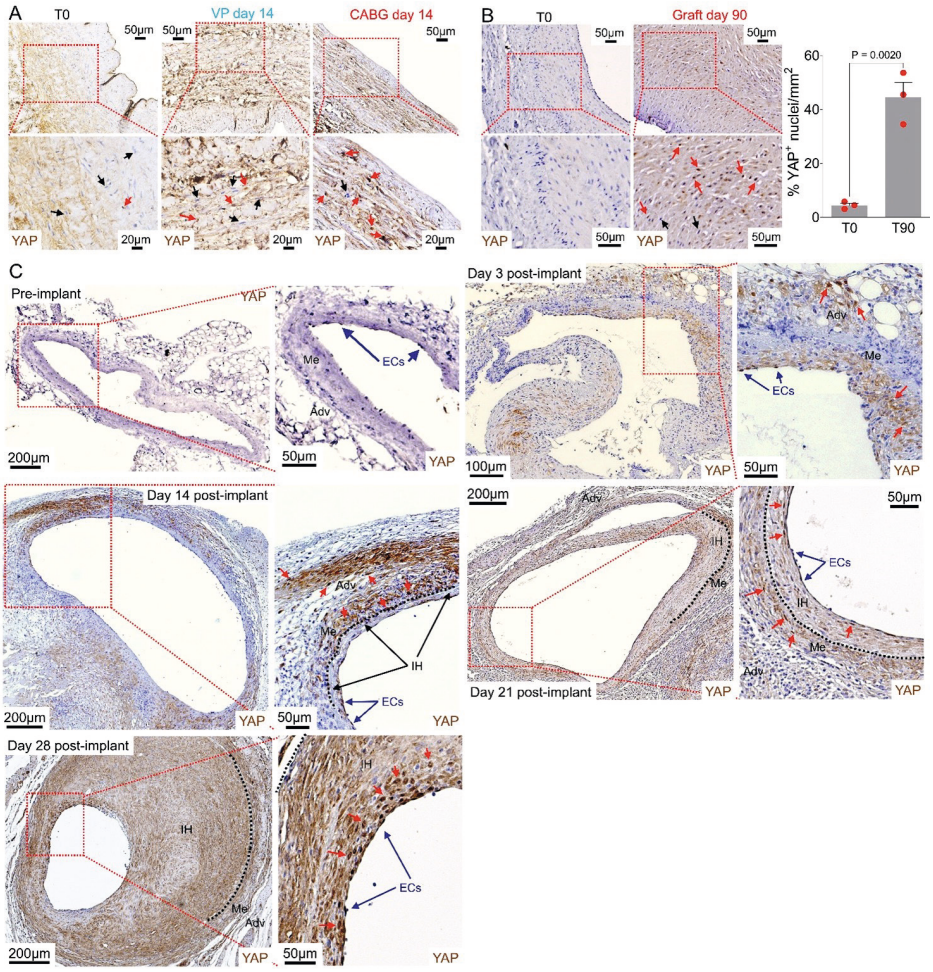

Figure 4. Dynamics of YAP upregulation in various models of vein arterialization.

(**A**) Exceeding SV conducts recovered from the surgery theatre were immediately processed for histology (T0) mounted and stimulated for two weeks in a bioreactor tailored to reproduce a flow with low-pressure, typical of the venous perfusion (VP), or the counter pulsed coronary circulation, typical of the coronary bypass (CABG). Pictures represent transversal sections of the vessels after unmounting from the bioreactors and following histological sectioning and YAP immunohistochemistry. Under these conditions, the cells in CABG-stimulated SVs exhibited a clear upregulation of YAP in the nuclei of the cells in the media (red arrows in the inset). (**B**) Transversal sections of pig SVs before and 90 days after implantation into carotids. As it is evident from the panels in freshly harvested SVs, the expression of YAP was negligible, while at 90 days, several cells in the vein wall were characterized by the presence of the co-factor in the nuclei (red arrows in the inset). Quantification of the cells was performed in three independent samples (bar graph on the right). The number of animals included in the quantification is indicated by the red circles overlapped to the bar graph. The significance was calculated by unpaired t-test. The *P* value of the test is indicated above the significance line. (**C**) The upregulation of YAP in a model of vena cava into carotid interposition in mice was also tested at different times. The pictures show transversal section of pre-implant or post-

implant vena cava immunostained with YAP-specific antibody. It is evident that before implantation, cells did not express the transcription factor. After implantation an increasing number of YAP+ cells were found either in the media (me) and the adventitia (Adv) of the vessel starting at 3 days. Some endothelial cells (ECs) also expressed the factor in line with the role of YAP as a mechanosensor of shear stress[83]. Note the increasing signal of nuclear YAP (red arrows) in cells of the hyperplastic intima (IH) starting at day 21 and culminating at day 28, in keeping with the lumen reduction.

Pharmacological blockade of YAP reduces migratory activity and fibrotic differentiation in responses to TGF-β/TSP-1 pathway.

We showed previously that pharmacological inhibition of YAP by Verteporfin (VTP), an FDA-approved inhibitor of the interaction between YAP/TAZ and DNA-binding proteins TEADs[40], reduces the expression of YAP-dependent targets in human valve interstitial cells[21] and, at least in part, prevents the mechanical- dependent fibrotic remodeling of the infarcted heart[20]. We therefore assessed the effect of the drug in human SVPs to decrease expression of canonical YAP targets *CTGF*, *CYR61* and *ANKRD1*. The observed decrease in expression of YAP targets confirmed pharmacological inhibition of YAP by VTP, which was independent of cytoskeleton tensioning, as shown by the presence of well-structured stress fibers in VTP-treated samples (**Figure S3**). Interestingly, treatment with VTP also partly inhibited expression of YAP, in line with existing literature[41], and reduced the migratory activity compared to controls (**Figure 5A**). This reduction coincided with a decrease in the expression of CD47 - one of the cellular receptors engaged in SVP migration against TSP-1 gradients[14], and a decrease in the number of focal adhesion contacts, as determined by immunofluorescence with anti-vinculin antibodies (**Figure 5B**). In order to find a mechanistic link between YAP and the TGF-β signaling, we hypothesized that YAP directly interacts with SMAD nuclear factors to upregulate expression of genes related to cell proliferation and SMC differentiation[42]. To verify this hypothesis, we first performed a proximity ligation assay (PLA) to assess a possible interaction of YAP and phospho-SMAD3 (pSMAD3), and then assessed expression of various genes and gene products by RT- qPCR and analyzed the cellular supernatants. As shown in **Figure 5C**, PLA clearly indicated the physical interaction of YAP and pSMAD3 in the nuclei of cells treated with TGF-β/TSP-1 combination, while the presence of VTP reduced the PLA signal to the level of controls, suggesting a direct involvement of YAP in TGF-β signaling. RT-qPCR performed on RNA extracted from SVPs showed that a number of genes relevant for VGD pathologic progression[43,44] were upregulated in the presence of the TGF-β/TSP-1 combination and were reduced by VTP. This included expression of Fibronectin (*FN*), *ACTA-2* (αSMA), and TSP-1 (*THBS1*) (**Figure 5D**). Upregulation of collagen – another important effector of fibrosis and VGD progression[45] – was also assessed both at the transcriptional and proteomic level, using RT-qPCR and dosage in cells culture supernatant, respectively (**Figure 5E**). Moreover, the upregulation of Collagen was inhibited by VTP, indicating a direct role of YAP in fibrotic/SMC commitment of SVPs induced by TGF-β signaling.

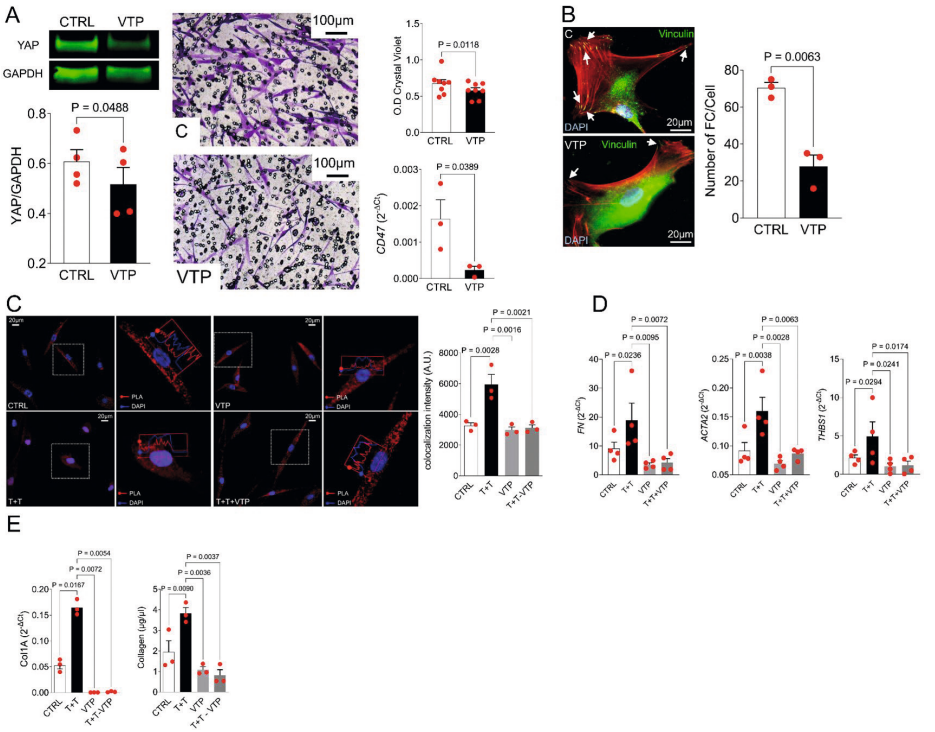

Figure 5. Interference with YAP transcriptional activity reduces sensitivity to TGF-β/TSP-1 signaling.

(**A**) Treating cells with Verteporfin (VTP) reduces expression of the transcriptional cofactor and migratory activity of human SVPs in transwells. On the top left of the panel it is represented a western blotting analysis of SVPs treated with VTP. Quantification of the western analysis is shown below. In the center of the panel there is a representative image of the migration assay performed in traswells with control and VTP-treated SVPs; the relative quantification is in the top right. VTP also downregulated expression of CD47, one of the main TSP-1 receptors that we already demonstrated to be relevant for migration of these cells[14]. (**B**) VTP reduces the amount of the focal adhesion contacts in SVPs. On the left of the panel a representative image of control cells showing a high number of vinculin-stained focal contacts (arrows). VTP inhibited significantly formation of focal contacts/cells, as shown in the bar graph. (**C**) Proximity ligand assay (PLA) performed with YAP and pSMAD3-specific antibodies. The proximity of the two transcriptional cofactors was followed by quantifying the red signal in the nuclei of control cells and cells treated with TGF-β, TSP-1 and the TGF- β/TSP-1 combination (T+T; see the fluorescence profiles overlapped to the nuclei of the cells). As it is evident from the representative images, the red signal was significantly elevated in cells treated with the T+T combination (bar graph on the right). This increase was reverted by VTP, indicating a functional cooperation of TGF-β and TSP-1 with nuclear signaling by YAP. (**D - E**) The TGF-β/TSP-1 combination also elevated the RNA expression of key fibrotic/myofibroblasts markers including Fibronectin (*FN*) *ACTA-2* (encoding for αSMA) and TSP-1 itself (*THBS1*). The combination also elevated the expression, either mRNA and secretion of collagen 1. In all cases the addition of VTP reduced to control levels the expression of these markers. Statistical comparisons were performed by pairwise student's t-test in panels **A** and **B** and by one- way Anova (repeated measures) with Tukey post-hoc in panels **C**, **D** and **E**. In all graphs, red dots overlapped to the bars indicate the result of each experiment performed in independent cell lines. The *P* values of the adopted statistical tests are indicated above the significance lines.

VTP improves vein graft remodeling by inhibiting intraplaque angiogenesis and the fibroproliferative response in vivo.

To test the therapeutic potential of VTP to improve vein graft remodeling in vivo, hypercholesteremic APOE*3-Leiden mice underwent venous bypass surgery (**Figure 6**). Treatment with VTP was initiated at 10 days after surgery – prior to the upregulation of YAP at 14 days (t14) (**Figure 4C**) – and maintained until sacrifice at day 28 (t28) post-surgery. VTP treatment was well tolerated, no apparent differences in behavior or wound healing were observed and bodyweight was similar between VTP and vehicle (**Figure S4**). Vein graft remodeling was longitudinally assessed using ultra-high frequency ultrasound. From t7 to t28, lumen area was slightly, and non-significantly, increased upon VTP treatment compared to minor decrease in the vehicle-group. In addition, wall area increased significantly during the same period, and this was in part inhibited by VTP (**Figure 6C**). In-depth analysis of the vessel wall on histology revealed that VTP determined a reduction in the ratio between the areas occupied by the intima (I) and the media (M) in the transversal sections (I/M ratio), indicating improved vein graft remodeling (**Figure 6A, C**). To evaluate whether VTP affected plaque stability, cellular compositional analysis on the vein grafts was performed. In line with our in vitro results, expression of ACTA2 (αSMA) was decreased by VTP (**Figure 6B, C**). Due to the critical role of YAP in endothelial cells we finally explored if VTP inhibited intraplaque angiogenesis, a hallmark of unstable atherosclerotic plaques. Plaque angiogenesis is in fact hardly observed in naïve murine atherosclerosis, but it a unique feature that is observed in our atherosclerotic vein graft model[46]. The number of neovessels/mm^2 was significantly reduced by VTP compared to vehicle. Moreover, VTP increased ACTA2 coverage of these neo-vessels indicating improved neo-vessel maturation (**Figure 6B, C**). Finally, given the involvement of TSP-1 in SV mechanical-dependent arterialization[14], we quantified the TSP-1$^+$ vein graft area. Vein grafts of VTP-treated mice exhibited significantly lower staining, indicating, in line with *in vitro* results (**Figures 6D**), a reduction in the expression of the matricellular protein and, hence, intra-graft TGF-β signaling. VTP also reduced systemic IL6 levels, indicative of a lower systemic inflammation[47] and, hence, to reduced pathological vein graft remodeling.

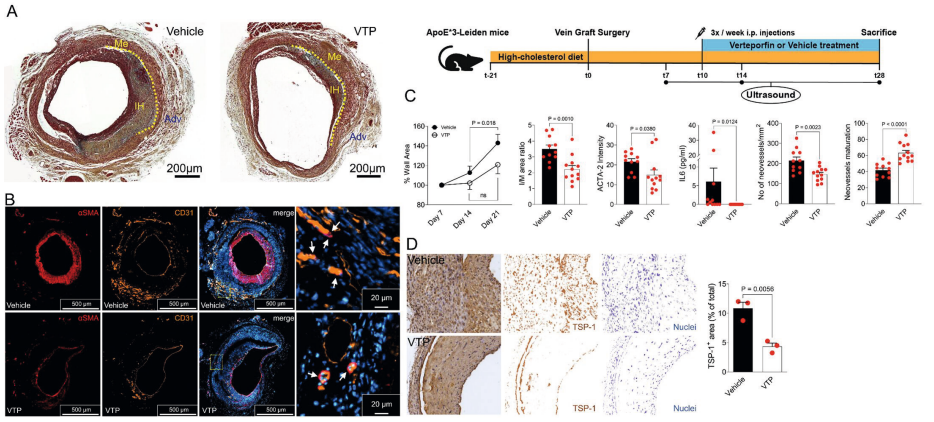

Figure 6. In vivo administration of VTP blunts progression of vein graft disease in mice.

(**A**) On the right side of the panel it is indicated the experimental protocol that was used in out in vivo approach. ApoE*3-Leiden mice were subjected to a high fat diet for 21 days prior to the surgery. After vena cava into carotid interposition, each mouse was monitored by ultrasound at day 7, 10, 14 and 21 after surgery. The intra-peritoneal administration of VTP (or vehicle as a control) started at day 10 after surgery. Sacrifice of mice and harvesting of biological material (veins, blood) occurred at day 28 after surgery. The two micrographs on the left show a low magnification of the transversal sections of mouse arterialized veins at 28 days post implant into carotids. Histological sections were stained with Movat pentachrome solution. In mice injected with control solution (vehicle) it is evident the presence of an abundant accumulation of intima (IH) and a secondary atherosclerotic plaque, well separated from the pre-existing media (Me). Systemic administration of VTP attenuated intima hyperplasia and, at least in part, reduced the formation of the plaques. (**B**) The micrographs show an immunofluorescence staining of the veins with antibodies specific for αSMA (red staining) and CD31 (yellow staining). As shown in the pictures, injection of VTP reduced the amount of the αSMA^+ cells in the vein wall and promoted maturation of the neo-vasculature present in neointima, indicative of reduced atherosclerosis, as shown by the higher number of vessels characterized by coverage of $CD31^+$ endothelial layer by αSMA^+ cells (compare the structure of these vessels in control vs. VTP-treated veins). (**C**) Quantification of vessel morphometry (% wall area, Intima/Media ratio), αSMA (ACTA2) intensity, circulating IL6 (pg/ml blood), vessel neoformation (density/mm^2) and vessel maturation (% of vessels covered by SMCs). (**D**) VTP significantly reduces the expression of TSP-1. The micrographs indicate the immunohistochemistry of the explanted vein grafts in control and VTP-injected mice. It is evident the reduction in the positive area in treated mice compared to controls (quantification in the bar graph on the right). Data in bar graphs were compared by unpaired t-test. In all graphs, red dots overlapped to the bars indicate the result of each experiment performed in independent animals. The *P* values of pairwise t-test are indicated above the significance lines

DISCUSSION

The problem of the maladaptive remodeling of venous coronary artery bypasses is known since the first follow up studies in the early '70s [49]. Since then, it was hypothesized that the damage caused during graft harvesting/preparation and the subsequent exposure to an unphysiological flow/pressure regimen is one of the major causes of the remodeling, in cooperation with other important factors like inflammation, hypercholesterolemia and hypertension[5]. While various strategies have been set to improve vein grafts patency, such as adoption of external stenting[50], use of 'no touch' harvesting procedures[51], storage of the vessel in protective buffers during the time of exposure outside the body of patients[52], the progressive occlusion of the venous grafts is still a major problem exposing patients to recurrence of ischemia[53].

Various studies have been conducted to identify the cellular and the molecular determinants of vein graft failure, and players such as metalloproteases and cell cycle genes were identified and validated in animal models using, for example, gene therapy approaches[11,54]. Some of the most promising results, at least in preclinical models, were obtained with transfer of TIMP-3[55], p53[56] and eNOS[57] genes. By contrast, the only clinical trial performed so far (the PREVENT trial58), based on treating the grafts with E2F decoy Edifoligide - have not met the expectation in terms of reduction of the disease[59,60]. Other interesting targets such as miR 2161 or inflammatory mediators (e.g. MCP-1/CCL2 chemokine[62]; Toll-like receptors[63]) have been finally identified in preclinical studies, but their significance is not yet consolidated clinically.

Involvement of a YAP/TGF-β signaling network in mechanical pathologic programming of SVPs

The saphenous conduits are living vessels that are removed from their natural bed to bypass the obstructions present in the coronary tree. Apart from endothelial cells important for vascular permeability and SMCs important form the maintenance of the vascular tone, other cell types are present in the intact vessel structure. SVPs are normally associated to vasa vasorum, from which they can be isolated as a $CD34^+$/$NG2^+$/$CD31^-$ cells[16]. While the main function of these cells is to maintain vascular homeostasis, their potential pathogenetic role has been also highlighted, with the evidence that they can be activated giving rise to fibrotic cells undergoing epigenetic modifications[15]. Using bioreactors tailored to expose human SVs to pressure or flow/pressure regimens typical of the coronary circulation, we have shown in various publications that the pulsatile stress to which the SV grafts are subjected during arterialization causes extensive morphological remodeling and activates a TGF-β-dependent signaling mediated by TSP-1; this matricellular factor is likely involved in the recruitment of adventitial progenitors[13,14,64,65]. In the present study, we aimed to contextualize the effects of mechanical forces on the pathologic programming of these cells, when exposed to a uniaxial strain (10% elongation) cyclic stimulation. This condition corresponds bona fide to the mechanical solicitation that cells receive in

the SV wall according to a numerical modeling of the radial strain associated to the counter-pulsed coronary flow in the grafts[14]. By whole genome transcriptomics and bioinformatics, we found numerous differentially expressed genes, and obtained a clear indication on transcriptional networks that may be involved in cell/extracellular matrix interactions, proliferation and crosstalk with the TGF-β signaling (**Figure 1**). Our attention was also directed to assess whether, in analogy with cardiac fibroblasts[20,26], the mechanical sensing of SVPs also involved the participation of components of the so-called Hippo transcriptional pathway[18]. Particular care was dedicated to assess a functional convergence of YAP (the most investigated Hippo transcriptional co-factor) with nuclear signaling downstream of TGF-β and the relationship with TEADs, the canonical cognate DNA binding proteins of the YAP/TAZ complex[66,67]. Our results clearly indicated mechanical-dependent modulation of genes represented as canonical YAP targets (CTGF, CYR61 and ANKRD1) and encoding for TGF-β transcriptional effectors (SMAD2/7) (**Figure 1D, G**). This regulation likely involved the F-actin cytoskeleton, as demonstrated by the reversible downregulation of the YAP targets by treating SVPs with FRSK, an activator of the cAMP/PKA pathway (**Figure 2A, B**)[32,68], and the cooperation of TEAD4 as a transcriptional co-factor, as assessed by bioinformatics (**Figure 3A, B**). The role of YAP in myofibroblast differentiation of human SVPs was further contextualized in the light of our previous findings showing that mechanical strain amplifies the effects of TGF-β through the release of TSP-1 from SMCs of the SV, as a result of a contractile to a secretory phenotype switch[14]. In particular, the combination of soluble TSP-1 and TGF-β enhanced the YAP nuclear signaling compared to the single treatments (**Figure 3C**), and this increased cellular proliferation and expression of SM22α (**Figure 3D**), ACTA2, FN, TSP1, Collagen1 (**Figure 5D, E**) and, finally, the physical association with pSMAD3 in the nuclei of the treated cells (**Figure 5C**). In line with findings from other groups in different model systems showing cooperation of YAP with components of the TGF-β signaling (in particular SMAD2/3 nuclear proteins) in endothelial-mesenchymal transition[69], or arterial stiffening[70], our data consolidate the role of YAP as a transcriptional co-factor with crucial roles in integration of mechanical and fibrotic signaling in cardiovascular pathologies[71].

In vivo blockade of YAP reduces vein graft disease

On the basis of our previous findings suggesting that YAP is involved in strain-dependent activation of cardiac fibroblasts in the ischemic heart[20], we investigated the expression of the transcriptional co-factor in three independent models of vein arterialization (**Figure 4**). In a first model, realized with a bioreactor able to mimic the flow/pressure patterns typical of the coronary circulation[13,14], we arterialized ex vivo human SV segments for up to 14 days. In a second approach, we performed a gold standard large animal model of bypass failure realized by interposing the SV into carotids in pigs with a 90 days follow-up[40]. Finally, we adopted a mouse model of vena cava into carotid interposition in hypercholesterolemic mice with a

follow-up to 28 days[23]. In all these models, although with different dynamics and efficiency, the localization of YAP in the nuclei of cells in the medial layer increased. Remarkably, as shown in the panels in **Figure 4**, the nuclear localization of the factor was pronounced preferentially in endothelial cells lining the lumen[72] and cells that had an elongated nuclear shape, similar to what we already observed in the heart of mice, where the fibroblasts are exposed to compression forces generated by the distribution of the radial strain[20]. We then aimed to modulate YAP signaling in vivo and reduce the molecular translation of the mechanical cues. To achieve this aim we employed transplantation of vena cava into carotids in hypercholesterolemic mice[23] and administered VTP, a drug that can be used in non photodynamic inhibition of the YAP/TAZ/TEADs complexes transcriptional function[41,73]. Longitudinal follow-up of vein graft remodeling using ultra high frequency ultrasound clearly evidenced a stepwise increase in the wall area and this, as shown by the images in Figure 6, involved extensive intima hyperplasia in control animals. Interestingly, these zones were the ones in which the cells expressed high levels of αSMA (**Figure 6B**) and TSP-1 (**Figure 6D**), consistent with a myofibroblast and secretory phenotype. Administration of VTP reduced this stepwise increase and prevented accumulation of αSMA^{+} cells in the sub intimal layer. This was accompanied by a remarkable inhibition of vessel wall remodeling (as assessed by reduction of the intima/media ratio), and of the area of the vein wall containing TSP-1^{+} cells (**Figure 6 C, D**). Finally, VTP treatment also drastically reduced the presence of IL-6 in peripheral blood, suggestive of reduced inflammation[74,75], and suppressed intraplaque angiogenesis whilst concomitantly enhancing the maturation of these newly formed vessels, thus improving plaque stability[47,76,77]. This warrants pharmacological YAP targeting as a new strategy to reduce myo-fibroproliferative response and adverse vein graft remodeling in less exploratory and more preclinically-oriented studies.

CONCLUSIONS

In the occurrence of coronary transplantation, the cells residing in the wall of the SV grafts (e.g., pre-existing, ECs, SMCs and SVPs), are subjected to a sudden increase of mechanical forces (e.g. shear stress, longitudinal and transversal wall strain)[78]. These forces have been mechanistically connected to progression of VGD. For example, we have found that exposure of human SV to a wall strain typical of the coronary-like flow/pressure pattern triggers a fibrotic process mediated by the TGF-β/TSP-1 signaling[14,65]. In this manuscript, we show that mechanical signaling induces a fibrotic evolution of SVPs involving the differential expression of several gene pathways connected to extracellular matrix remodeling, and cellular/matrix interactions. Our data also suggest that there is a synergistic effect of mechanical forces and matricellular signaling elicited by the TGF-β/TSP-1 combination. This is showed by drastic increase of SMCs/fibrotic markers (FN, ACTA-2, TSP-1, Collagen) expression when SVPs were treated with a combination of the two fibrotic factors

onto rigid substrates, and by the crucial role of YAP as a mechanically activated transcriptional co factor in their phenotypic transformation.

The recent pre-clinical success of external stenting to reducing the impact of the unphysiological wall mechanics to consequently reduce adverse vein graft remodeling, highlights that limiting transmission of the excess strain is crucial to reduce excessive cell proliferation and, hence, retard bypass failure[79,80]. This protective effect is mediated through modulation of YAP signaling81 and provides compelling evidence for the so called "mechano-therapeutic" approach as a new avenue to prevent maladaptive remodeling of cardiovascular tissues[71]. Our results indicate that this approach is practicable, even though particular care will have to be dedicated to choose an appropriate release system of the drug locally to the graft. In summary our evidences suggest that reducing mechanically-induced activation of vein resident progenitors by pharmacologically targeting YAP could have beneficial effects on reducing intima hyperplasia by targeting vein resident progenitor as precursors of activated fibroblasts and, potentially, SMCs. While this is a potentially different approach compared to gene therapy that has been historically employed to target SMCs hyperplasia[82], it also provides new opportunities for development of new devices such as nanotechnologies or materials endowed with a slow-release drug potential to maximize therapeutic effects. Various options are available such as pretreating the grafts with the drug prior to be re implanted in the patient's body (such in existing gene therapy trials), or to release the drug by active or passive support systems (e.g. nanoparticles, drug-releasing external stents, drug containing hydrogels)[83]. We anticipate that these strategies might be helpful to minimize the side effects of the drug systemic administration, and localize the therapeutic intervention to the grafts.

STUDY LIMITATIONS

The present study is a proof of concept that inhibition of YAP with VTP may have an efficacy against the maladaptive remodeling of the arterialized vein causes by sensing of mechanical forces. Although in line with our previous findings in the infarcted heart[20], this was mechanistically related to the reduction of the TGF-β-dependent transcriptional pathways in cultured SVPs, the inhibition of vascular remodeling in vivo could be caused by cumulation of unrelated effects such as inhibition of inflammation[84], inhibition of proliferation and enhancement of apoptosis85 or, finally, a reduction in OXPHOS activity[86]. More directed cell-specific YAP targeting approaches should be endeavored in the future to address this important mechanistic point. Another limitation of the present study is the modality of VTP administration in the animal model of vein graft administration. We are aware of the disadvantages that systemic injection of the drug may cause, given its pleiotropic action. In this regard, we anticipate that exposure of the SV to the drug or mixing the drug with a polymer that could be used to slowly release it on the adventitial side might increase the

efficiency of the treatment and minimize the side effects. This feasibility of the last option has been already shown in the literature[81] and we are presently implementing systems to pursue it.

Author disclosure
The Authors declare no conflicts of interest.

Supplemental Material
Supplemental Methods, Tables S1 – S3, Figures S1 – S4, Datasets S1-S5, References 87 – 96.

Funding
The present research was granted by an institutional research funding issued by Italian Ministry of Health (Ricerca Corrente, projects no 2764157, 2771985, 2775037) to MP. FM is supported by the Italian Ministry of Health ("Ricerca Corrente 2023", RF-2019-12368521, POS T4 CAL.HUB.RIA, cod. T4-AN-09), by Telethon Foundation (#4462 GGP19035A), AFM-Telethon (# 23054), and by the EU-Next Generation EU- NRRP M6C2 – Inv.2.1 PNRR-MAD-2022-12375790. MdV was supported by a grant funded by the Rembrandt Institute for Cardiovascular Science.

REFERENCES

1. Gaudino M, Benedetto U, Fremes S, Ballman K, Biondi-Zoccai G, Sedrakyan A, Nasso G, Raman J, Buxton B, Hayward PA, et al. Association of Radial Artery Graft vs Saphenous Vein Graft With Long-term Cardiovascular Outcomes Among Patients Undergoing Coronary Artery Bypass Grafting: A Systematic Review and Meta-analysis. *JAMA : the journal of the American Medical Association*. 2020;324:179-187. doi: 10.1001/jama.2020.8228
2. Xenogiannis I, Zenati M, Bhatt DL, Rao SV, Rodes-Cabau J, Goldman S, Shunk KA, Mavromatis K, Banerjee S, Alaswad K, et al. Saphenous Vein Graft Failure: From Pathophysiology to Prevention and Treatment Strategies. *Circulation*. 2021;144:728-745. doi: 10.1161/CIRCULATIONAHA.120.052163
3. Arsalan M, Mack MJ. Coronary Artery Bypass Grafting Is Currently Underutilized. *Circulation*. 2016;133:1036-1045. doi: 10.1161/CIRCULATIONAHA.115.018032
4. Farber A, Menard MT, Conte MS, Kaufman JA, Powell RJ, Choudhry NK, Hamza TH, Assmann SF, Creager MA, Cziraky MJ, et al. Surgery or Endovascular Therapy for Chronic Limb-Threatening Ischemia. *The New England journal of medicine*. 2022;387:2305-2316. doi: 10.1056/NEJMoa2207899
5. Caliskan E, de Souza DR, Boning A, Liakopoulos OJ, Choi YH, Pepper J, Gibson CM, Perrault LP, Wolf RK, Kim KB, et al. Saphenous vein grafts in contemporary coronary artery bypass graft surgery. *Nat Rev Cardiol*. 2020;17:155-169. doi: 10.1038/s41569-019-0249-3
6. de Vries MR, Quax PHA. Inflammation in Vein Graft Disease. *Frontiers in Cardiovascular Medicine*. 2018;5. doi: 10.3389/fcvm.2018.00003
7. de Vries MR, Simons KH, Jukema JW, Braun J, Quax PHA. Vein graft failure: from pathophysiology to clinical outcomes. *Nature Reviews Cardiology*. 2016;13:451. doi: 10.1038/nrcardio.2016.76
8. Hu Y, Xu Q. Adventitial Biology: Differentiation and Function. *Arteriosclerosis, Thrombosis, and Vascular Biology*. 2011;31:1523-1529. doi: 10.1161/atvbaha.110.221176
9. Torsney E, Hu Y, Xu Q. Adventitial progenitor cells contribute to arteriosclerosis. *Trends Cardiovasc Med*. 2005;15:64-68. doi: 10.1016/j.tcm.2005.02.003
10. Hu Y, Zhang Z, Torsney E, Afzal AR, Davison F, Metzler B, Xu Q. Abundant progenitor cells in the adventitia contribute to atherosclerosis of vein grafts in ApoE-deficient mice. *The Journal of clinical investigation*. 2004;113:1258-1265. doi: 10.1172/jci19628
11. Southerland KW, Frazier SB, Bowles DE, Milano CA, Kontos CD. Gene therapy for the prevention of vein graft disease. *Transl Res*. 2013;161:321-338. doi: 10.1016/j.trsl.2012.12.003
12. Newby AC. Coronary vein grafting: the flags keep waving but the game goes on. *Cardiovasc Res*. 2013;97:193-194. doi: 10.1093/cvr/cvs351
13. Piola M, Ruiter M, Vismara R, Mastrullo V, Agrifoglio M, Zanobini M, Pesce M, Soncini M, Fiore GB. Full Mimicking of Coronary Hemodynamics for Ex-Vivo Stimulation of Human Saphenous Veins. *Ann Biomed Eng*. 2017;45:884-897. doi: 10.1007/s10439-016-1747-7
14. Garoffolo G, Ruiter MS, Piola M, Brioschi M, Thomas AC, Agrifoglio M, Polvani G, Coppadoro L, Zoli S, Saccu C, et al. Coronary artery mechanics induces human saphenous vein remodelling via recruitment of adventitial myofibroblast-like cells mediated by Thrombospondin-1. *Theranostics*. 2020;10:2597-2611. doi: 10.7150/thno.40595
15. Gubernator M, Slater SC, Spencer HL, Spiteri I, Sottoriva A, Riu F, Rowlinson J, Avolio E, Katare R, Mangialardi G, et al. Epigenetic profile of human adventitial progenitor cells correlates with therapeutic outcomes in a mouse model of limb ischemia. *Arterioscler Thromb Vasc Biol*. 2015;35:675-688. doi: 10.1161/atvbaha.114.304989

16. Campagnolo P, Cesselli D, Al Haj Zen A, Beltrami AP, Kränkel N, Katare R, Angelini G, Emanueli C, Madeddu P. Human adult vena saphena contains perivascular progenitor cells endowed with clonogenic and proangiogenic potential. *Circulation*. 2010;121:1735-1745. doi: 10.1161/circulationaha.109.899252
17. Dupont S, Morsut L, Aragona M, Enzo E, Giulitti S, Cordenonsi M, Zanconato F, Le Digabel J, Forcato M, Bicciato S, et al. Role of YAP/TAZ in mechanotransduction. *Nature*. 2011;474:179-183. doi: 10.1038/nature10137
18. Piccolo S, Dupont S, Cordenonsi M. The biology of YAP/TAZ: hippo signaling and beyond. *Physiological reviews*. 2014;94:1287-1312. doi: 10.1152/physrev.00005.2014
19. Schroer AK, Merryman WD. Mechanobiology of myofibroblast adhesion in fibrotic cardiac disease. *J Cell Sci*. 2015;128:1865-1875. doi: 10.1242/jcs.162891
20. Garoffolo G, Casaburo M, Amadeo F, Salvi M, Bernava G, Piacentini L, Chimenti I, Zaccagnini G, Milcovich G, Zuccolo E, et al. Reduction of Cardiac Fibrosis by Interference With YAP-Dependent Transactivation. *Circ Res*. 2022;131:239-257. doi: 10.1161/CIRCRESAHA.121.319373
21. Santoro R, Scaini D, Severino LU, Amadeo F, Ferrari S, Bernava G, Garoffolo G, Agrifoglio M, Casalis L, Pesce M. Activation of human aortic valve interstitial cells by local stiffness involves YAP-dependent transcriptional signaling. *Biomaterials*. 2018;181:268-279. doi: 10.1016/j.biomaterials.2018.07.033
22. Nardone G, La Cruz JOD, Vrbsky J, Martini C, Pribyl J, Skladal P, Pesl M, Caluori G, Pagliari S, Martino F, et al. YAP regulates cell mechanics by controlling focal adhesion assembly. *Nature Communications*. 2017;8:15321. doi: 10.1038/Ncomms15321
23. Lardenoye JH, de Vries MR, Lowik CW, Xu Q, Dhore CR, Cleutjens JP, van Hinsbergh VW, van Bockel JH, Quax PH. Accelerated atherosclerosis and calcification in vein grafts: a study in APOE*3 Leiden transgenic mice. *Circ Res*. 2002;91:577-584. doi: 10.1161/01.res.0000036901.58329.d7
24. Thomas AC, Wyatt MJ, Newby AC. Reduction of early vein graft thrombosis by tissue plasminogen activator gene transfer. *Thrombosis and haemostasis*. 2009;102:145-152. doi: 10.1160/th08-11-0772
25. Maselli D, Garoffolo G, Cassanmagnago GA, Vono R, Ruiter MS, Thomas AC, Madeddu P, Pesce M, Spinetti G. Mechanical Strain Induces Transcriptomic Reprogramming of Saphenous Vein Progenitors. *Front Cardiovasc Med*. 2022;9:884031. doi: 10.3389/fcvm.2022.884031
26. Ugolini GS, Rasponi M, Pavesi A, Santoro R, Kamm R, Fiore GB, Pesce M, Soncini M. On-chip assessment of human primary cardiac fibroblasts proliferative responses to uniaxial cyclic mechanical strain. *Biotechnol Bioeng*. 2016;113:859-869. doi: 10.1002/bit.25847
27. Piersma B, Bank RA, Boersema M. Signaling in Fibrosis: TGF-beta, WNT, and YAP/TAZ Converge. *Front Med (Lausanne)*. 2015;2:59. doi: 10.3389/fmed.2015.00059
28. Zhao B, Wei X, Li W, Udan RS, Yang Q, Kim J, Xie J, Ikenoue T, Yu J, Li L, et al. Inactivation of YAP oncoprotein by the Hippo pathway is involved in cell contact inhibition and tissue growth control. *Genes Dev*. 2007;21:2747-2761. doi: 10.1101/gad.1602907
29. Aragona M, Panciera T, Manfrin A, Giulitti S, Michielin F, Elvassore N, Dupont S, Piccolo S. A Mechanical Checkpoint Controls Multicellular Growth through YAP/TAZ Regulation by Actin-Processing Factors. *Cell*. 2013;154:1047-1059. doi: 10.1016/j.cell.2013.07.042
30. Xiao Y, Hill MC, Li L, Deshmukh V, Martin TJ, Wang J, Martin JF. Hippo pathway deletion in adult resting cardiac fibroblasts initiates a cell state transition with spontaneous and self-sustaining fibrosis. *Genes Dev*. 2019;33:1491-1505. doi: 10.1101/gad.329763.119
31. Dey A, Varelas X, Guan KL. Targeting the Hippo pathway in cancer, fibrosis, wound healing and regenerative medicine. *Nature Reviews Drug Discovery*. 2020;19:480-494. doi: 10.1038/s41573-020-0070-z

32. Kimura TE, Duggirala A, Smith MC, White S, Sala-Newby GB, Newby AC, Bond M. The Hippo pathway mediates inhibition of vascular smooth muscle cell proliferation by cAMP. *J Mol Cell Cardiol*. 2016;90:1-10. doi: 10.1016/j.yjmcc.2015.11.024
33. Howe AK. Regulation of actin-based cell migration by cAMP/PKA. *Biochim Biophys Acta*. 2004;1692:159-174. doi: 10.1016/j.bbamcr.2004.03.005
34. Salvi M, Morbiducci U, Amadeo F, Santoro R, Angelini F, Chimenti I, Massai D, Messina E, Giacomello A, Pesce M, et al. Automated Segmentation of Fluorescence Microscopy Images for 3D Cell Detection in human- derived Cardiospheres. *Sci Rep*. 2019;9:6644. doi: 10.1038/s41598-019-43137-2
35. Mana-Capelli S, McCollum D. Angiomotins stimulate LATS kinase autophosphorylation and act as scaffolds that promote Hippo signaling. The Journal of biological chemistry. 2018;293:18230-18241. Doi: 10.1074/jbc.RA118.004187
36. Chen Y, Zhao X, Sun J, Su W, Zhang L, Li Y, Liu Y, Zhang L, Lu Y, Shan H, et al. YAP1/Twist promotes fibroblast activation and lung fibrosis that conferred by miR-15a loss in IPF. *Cell Death Differ*. 2019;26:1832- 1844. doi: 10.1038/s41418-018-0250-0
37. Fujii M, Toyoda T, Nakanishi H, Yatabe Y, Sato A, Matsudaira Y, Ito H, Murakami H, Kondo Y, Kondo E, et al. TGF-beta synergizes with defects in the Hippo pathway to stimulate human malignant mesothelioma growth. *J Exp Med*. 2012;209:479-494. doi: 10.1084/jem.20111653
38. Ebrahimighaei R, Sala-Newby GB, Hudson C, Kimura TE, Hathway T, Hawkins J, McNeill MC, Richardson R, Newby AC, Bond M. Combined role for YAP-TEAD and YAP-RUNX2 signalling in substrate-stiffness regulation of cardiac fibroblast proliferation. *Biochim Biophys Acta Mol Cell Res*. 2022;1869:119329. doi: 10.1016/j.bbamcr.2022.119329
39. Humeres C, Venugopal H, Frangogiannis NG. Smad-dependent pathways in the infarcted and failing heart. *Curr Opin Pharmacol*. 2022;64:102207. doi: 10.1016/j.coph.2022.102207
40. Thomas AC. Animal models for studying vein graft failure and therapeutic interventions. *Curr Opin Pharmacol*. 2012;12:121-126. doi: 10.1016/j.coph.2012.01.002
41. Gibault F, Corvaisier M, Bailly F, Huet G, Melnyk P, Cotelle P. Non-Photoinduced Biological Properties of Verteporfin. *Current medicinal chemistry*. 2016;23:1171-1184.
42. Wei L, Ma X, Hou Y, Zhao T, Sun R, Qiu C, Liu Y, Qiu Z, Liu Z, Jiang J. Verteporfin reverses progestin resistance through YAP/TAZ-PI3K-Akt pathway in endometrial carcinoma. *Cell Death Discov*. 2023;9:30. doi: 10.1038/s41420-023-01319-y
43. Szeto SG, Narimatsu M, Lu M, He X, Sidiqi AM, Tolosa MF, Chan L, De Freitas K, Bialik JF, Majumder S, et al. YAP/TAZ Are Mechanoregulators of TGF-β-Smad Signaling and Renal Fibrogenesis. *Journal of the American Society of Nephrology*. 2016;27:3117-3128. doi: 10.1681/asn.2015050499
44. Khan R, Agrotis A, Bobik A. Understanding the role of transforming growth factor-beta1 in intimal thickening after vascular injury. *Cardiovasc Res*. 2007;74:223-234. doi: 10.1016/j.cardiores.2007.02.012
45. Jiang Z, Tao M, Omalley KA, Wang D, Ozaki CK, Berceli SA. Established neointimal hyperplasia in vein grafts expands via TGF-beta-mediated progressive fibrosis. *American journal of physiology Heart and circulatory physiology*. 2009;297:H1200-1207. doi: 10.1152/ajpheart.00268.2009
46. Low EL, Baker AH, Bradshaw AC. TGFbeta, smooth muscle cells and coronary artery disease: a review. *Cellular signalling*. 2019;53:90-101. doi: 10.1016/j.cellsig.2018.09.004
47. de Vries MR, Parma L, Peters HAB, Schepers A, Hamming JF, Jukema JW, Goumans M, Guo L, Finn AV, Virmani R, et al. Blockade of vascular endothelial growth factor receptor 2 inhibits intraplaque haemorrhage by normalization of plaque neovessels. *J Intern Med*. 2019;285:59-74. doi: 10.1111/joim.12821

48. de Jong A, de Jong RCM, Peters EA, Arens R, Jukema JW, de Vries MR, Quax PHA. P300/CBP Associated Factor (PCAF) Deficiency Enhances Diet-Induced Atherosclerosis in ApoE3(*)Leiden Mice via Systemic Inhibition of Regulatory T Cells. *Front Cardiovasc Med*. 2020;7:604821. doi: 10.3389/fcvm.2020.604821
49. GRONDIN CM, MEERE C, CASTONGUAY Y, LEPAGE G, GRONDIN P. Progressive and Late Obstruction of an Aorto-Coronary Venous Bypass Graft. *Circulation*. 1971;43:698-702. doi: 10.1161/01.cir.43.5.698
50. Chen H, Wang Z, Si K, Wu X, Ni H, Tang Y, Liu W, Wang Z. External stenting for saphenous vein grafts in coronary artery bypass grafting: A meta-analysis. *Eur J Clin Invest*. 2023;53:e14046. doi: 10.1111/eci.14046
51. Elshafay A, Bendary AH, Vuong HT, Ahmed AR, Mokhtar MA, Soliman AL, Vuong NL, Bestawi IAE, Abdallah NA, Vu VT, et al. Does No-Touch Technique Better than Conventional or Intermediate Saphenous Vein Harvest Techniques for Coronary Artery Bypass Graft Surgery: a Systematic Review and Meta-analysis. *J Cardiovasc Transl Res*. 2018;11:483-494. doi: 10.1007/s12265-018-9832-y
52. Layton GR, Ladak SS, Abbasciano R, McQueen LW, George SJ, Murphy GJ, Zakkar M. The Role of Preservation Solutions upon Saphenous Vein Endothelial Integrity and Function: Systematic Review and UK Practice Survey. *Cells*. 2023;12. doi: 10.3390/cells12050815
53. Gaudino M, Sandner S, An KR, Dimagli A, Di Franco A, Audisio K, Harik L, Perezgrovas-Olaria R, Soletti G, Fremes SE, et al. Graft Failure After Coronary Artery Bypass Grafting and Its Association With Patient Characteristics and Clinical Events: A Pooled Individual Patient Data Analysis of Clinical Trials With Imaging Follow-Up. *Circulation*. 2023;148:1305-1315. doi: 10.1161/CIRCULATIONAHA.123.064090
54. Wang XW, Zhao XJ, Xiang XY. Gene therapy for vein graft failure. *Journal of cardiac surgery*. 2013;28:144-147. doi: 10.1111/jocs.12075
55. George SJ, Wan S, Hu J, MacDonald R, Johnson JL, Baker AH. Sustained reduction of vein graft neointima formation by ex vivo TIMP-3 gene therapy. *Circulation*. 2011;124:S135-142. doi: 10.1161/CIRCULATIONAHA.110.012732
56. Wan S, George SJ, Nicklin SA, Yim AP, Baker AH. Overexpression of p53 increases lumen size and blocks neointima formation in porcine interposition vein grafts. *Mol Ther*. 2004;9:689-698. doi: 10.1016/j.ymthe.2004.02.005
57. West NE, Qian H, Guzik TJ, Black E, Cai S, George SE, Channon KM. Nitric oxide synthase (nNOS) gene transfer modifies venous bypass graft remodeling: effects on vascular smooth muscle cell differentiation and superoxide production. *Circulation*. 2001;104:1526-1532. doi: 10.1161/hc3801.095693
58. Mann MJ, Whittemore AD, Donaldson MC, Belkin M, Conte MS, Polak JF, Orav EJ, Ehsan A, Dell'Acqua G, Dzau VJ. Ex-vivo gene therapy of human vascular bypass grafts with E2F decoy: the PREVENT single-centre, randomised, controlled trial. *Lancet*. 1999;354:1493-1498. doi: 10.1016/S0140-6736(99)09405-2
59. Lopes RD, Williams JB, Mehta RH, Reyes EM, Hafley GE, Allen KB, Mack MJ, Peterson ED, Harrington RA, Gibson CM, et al. Edifoligide and long-term outcomes after coronary artery bypass grafting: PRoject of Ex-vivo Vein graft ENgineering via Transfection IV (PREVENT IV) 5-year results. *Am Heart J*. 2012;164:379-386 e371. doi: 10.1016/j.ahj.2012.05.019
60. Alexander JH, Hafley G, Harrington RA, Peterson ED, Ferguson TB, Jr., Lorenz TJ, Goyal A, Gibson M, Mack MJ, Gennevois D, et al. Efficacy and safety of edifoligide, an E2F transcription factor decoy, for prevention of vein graft failure following coronary artery bypass graft surgery: PREVENT IV: a randomized controlled trial. *JAMA : the journal of the American Medical Association*. 2005;294:2446-2454. doi: 10.1001/jama.294.19.2446

61. McDonald RA, White KM, Wu J, Cooley BC, Robertson KE, Halliday CA, McClure JD, Francis S, Lu R, Kennedy S, et al. miRNA-21 is dysregulated in response to vein grafting in multiple models and genetic ablation in mice attenuates neointima formation. *Eur Heart J*. 2013;34:1636-1643. doi: 10.1093/eurheartj/eht105
62. Schepers A, Eefting D, Bonta PI, Grimbergen JM, de Vries MR, van Weel V, de Vries CJ, Egashira K, van Bockel JH, Quax PHA. Anti–MCP-1 Gene Therapy Inhibits Vascular Smooth Muscle Cells Proliferation and Attenuates Vein Graft Thickening Both In Vitro and In Vivo. *Arteriosclerosis, Thrombosis, and Vascular Biology*. 2006;26:2063-2069. doi: 10.1161/01.ATV.0000235694.69719.e2
63. Simons KH, de Vries MR, Peters HAB, Hamming JF, Jukema JW, Quax PHA. The protective role of Toll-like receptor 3 and type-I interferons in the pathophysiology of vein graft disease. *J Mol Cell Cardiol*. 2018;121:16-24. doi: 10.1016/j.yjmcc.2018.06.001
64. Piola M, Prandi F, Bono N, Soncini M, Penza E, Agrifoglio M, Polvani G, Pesce M, Fiore GB. A compact and automated ex vivo vessel culture system for the pulsatile pressure conditioning of human saphenous veins. *Journal of tissue engineering and regenerative medicine*. 2016;10:E204-215. doi: 10.1002/term.1798
65. Prandi F, Piola M, Soncini M, Colussi C, D'Alessandra Y, Penza E, Agrifoglio M, Vinci MC, Polvani G, Gaetano C, et al. Adventitial vessel growth and progenitor cells activation in an ex vivo culture system mimicking human saphenous vein wall strain after coronary artery bypass grafting. *PLoS One*. 2015;10:e0117409. doi: 10.1371/journal.pone.0117409
66. Liu F, Wang X, Hu G, Wang Y, Zhou J. The Transcription Factor TEAD1 Represses Smooth Muscle-specific Gene Expression by Abolishing Myocardin Function. *Journal of Biological Chemistry*. 2014;289:3308-3316. doi: 10.1074/jbc.M113.515817
67. Schlegelmilch K, Mohseni M, Kirak O, Pruszak J, Rodriguez JR, Zhou D, Kreger Bridget T, Vasioukhin V, Avruch J, Brummelkamp Thijn R, et al. Yap1 Acts Downstream of α-Catenin to Control Epidermal Proliferation. *Cell*. 2011;144:782-795. doi: 10.1016/j.cell.2011.02.031
68. Ebrahimighaei R, McNeill MC, Smith SA, Wray JP, Ford KL, Newby AC, Bond M. Elevated cyclic-AMP represses expression of exchange protein activated by cAMP (EPAC1) by inhibiting YAP-TEAD activity and HDAC-mediated histone deacetylation. *Bba-Mol Cell Res*. 2019;1866:1634-1649. doi: 10.1016/j.bbamcr.2019.06.013
69. Savorani C, Malinverno M, Seccia R, Maderna C, Giannotta M, Terreran L, Mastrapasqua E, Campaner S, Dejana E, Giampietro C. A dual role of YAP in driving TGFbeta-mediated endothelial-to-mesenchymal transition. *J Cell Sci*. 2021;134. doi: 10.1242/jcs.251371
70. Liu Y, Li M, Lv X, Bao K, Yu Tian X, He L, Shi L, Zhu Y, Ai D. Yes-Associated Protein Targets the Transforming Growth Factor beta Pathway to Mediate High-Fat/High-Sucrose Diet-induced Arterial Stiffness. *Circ Res*. 2022;130:851-867. doi: 10.1161/CIRCRESAHA.121.320464
71. Pesce M, Duda GN, Forte G, Girao H, Raya A, Roca-Cusachs P, Sluijter JPG, Tschope C, Van Linthout S. Cardiac fibroblasts and mechanosensation in heart development, health and disease. *Nat Rev Cardiol*. 2023;20:309-324. doi: 10.1038/s41569-022-00799-2
72. Wang L, Luo JY, Li, B, Tian XY, Chen LJ, Huang Y, Liu Y, Deng D, Lau CW, Wan S et al. Integrin-YAP/TAZ/JNK cascade mediates atheroprotective effect of unidirectional shear flow. *Nature*. 2016;540:579-582. Doi: 10.1038/nature20602
73. Feng J, Gou J, Jia J, Yi T, Cui T, Li Z. Verteporfin, a suppressor of YAP-TEAD complex, presents promising antitumor properties on ovarian cancer. *OncoTargets and therapy*. 2016;9:5371-5381. doi: 10.2147/ott.s109979
74. Mia MM, Cibi DM, Abdul Ghani SAB, Song W, Tee N, Ghosh S, Mao J, Olson EN, Singh MK. YAP/TAZ deficiency reprograms macrophage phenotype and improves infarct healing and cardiac function after myocardial infarction. *PLoS Biol*. 2020;18:e3000941. doi: 10.1371/journal.pbio.3000941

75. de Jong A, Sier VQ, Peters HAB, Schilder NKM, Jukema JW, Goumans M, Quax PHA, de Vries MR. Interfering in the ALK1 Pathway Results in Macrophage-Driven Outward Remodeling of Murine Vein Grafts. *Front Cardiovasc Med*. 2021;8:784980. doi: 10.3389/fcvm.2021.784980
76. Baganha F, de Jong RCM, Peters EA, Voorham W, Jukema JW, Delibegovic M, de Vries MR, Quax PHA. Atorvastatin pleiotropically decreases intraplaque angiogenesis and intraplaque haemorrhage by inhibiting ANGPT2 release and VE-Cadherin internalization. *Angiogenesis*. 2021;24:567-581. doi: 10.1007/s10456-021- 09767-9
77. Parma L, Peters HAB, Sluiter TJ, Simons KH, Lazzari P, de Vries MR, Quax PHA. bFGF blockade reduces intraplaque angiogenesis and macrophage infiltration in atherosclerotic vein graft lesions in ApoE3*Leiden mice. *Sci Rep*. 2020;10:15968. doi: 10.1038/s41598-020-72992-7
78. Jackson ML, Bond AR, George SJ. Mechanobiology of the endothelium in vascular health and disease: in vitro shear stress models. *Cardiovasc Drugs Ther*. 2023;37:997-1010. doi: 10.1007/s10557-022-07385-1
79. Jeremy JY, Gadsdon P, Shukla N, Vijayan V, Wyatt M, Newby AC, Angelini GD. On the biology of saphenous vein grafts fitted with external synthetic sheaths and stents. *Biomaterials*. 2007;28:895-908. doi: 10.1016/j.biomaterials.2006.10.023
80. Mehta D, George SJ, Jeremy JY, Izzat MB, Southgate KM, Bryan AJ, Newby AC, Angelini GD. External stenting reduces long-term medial and neointimal thickening and platelet derived growth factor expression in a pig model of arteriovenous bypass grafting. *Nat Med*. 1998;4:235-239.
81. Yang Q, Lei D, Huang S, Yang Y, Jiang C, Shi H, Chen W, Zhao Q, You Z, Ye X. A novel biodegradable external stent regulates vein graft remodeling via the Hippo-YAP and mTOR signaling pathways. *Biomaterials*. 2020;258:120254. doi: 10.1016/j.biomaterials.2020.120254
82. Yla-Herttuala S, Baker AH. Cardiovascular Gene Therapy: Past, Present, and Future. *Mol Ther*. 2017;25:1095-1106. doi: 10.1016/j.ymthe.2017.03.027
83. Zhou Z, Chen W, Cao Y, Abdi R, Tao W. Nanomedicine-based strategies for the treatment of vein graft disease. Nat Rev Cardiol. 2024. doi: 10.1038/s41569-024 01094-y
84. Wang Y, Wang L, Wise JTF, Shi X, Chen Z. Verteporfin inhibits lipopolysaccharide-induced inflammation by multiple functions in RAW 264.7 cells. *Toxicology and applied pharmacology*. 2020;387:114852. doi: 10.1016/j.taap.2019.114852
85. Wei C, Li X. Verteporfin inhibits cell proliferation and induces apoptosis in different subtypes of breast cancer cell lines without light activation. BMC Cancer. 2020;20:1042. doi: 10.1186/s12885-020-07555-0
86. Kuramoto K, Yamamoto M, Suzuki S, Sanomachi T, Togashi K, Seino S, Kitanaka C, Okada M. Verteporfin inhibits oxidative phosphorylation and induces cell death specifically in glioma stem cells. *FEBS J*. 2020;287:2023-2036. doi: 10.1111/febs.15187
87. Dobin A, Davis CA, Schlesinger F, Drenkow J, Zaleski C, Jha S, Batut P, Chaisson M, Gingeras TR. STAR: ultrafast universal RNA-seq aligner. Bioinformatics (Oxford, England). 2013;29:15-21. doi: 10.1093/bioinformatics/bts635
88. Langmead B, Salzberg SL. Fast gapped-read alignment with Bowtie 2. Nature methods. 2012;9:357-359. doi: 10.1038/nmeth.1923
89. Liao Y, Smyth GK, Shi W. featureCounts: an efficient general purpose program for assigning sequence reads to genomic features. Bioinformatics (Oxford, England). 2014;30:923-930. doi: 10.1093/bioinformatics/btt656
90. 2014;30:923-930. doi: 10.1093/bioinformatics/btt656 Chiesa M, Colombo GI, Piacentini L. DaMiRseq-an R/Bioconductor package for data mining of RNA-Seq data: normalization, feature selection and classification. Bioinformatics (Oxford, England) 2018;34:1416-1418. Doi: 10.1093/bioinformatics/btx795

91. Smyth GK, Michaud J, Scott HS. Use of within-array replicate spots for assessing differential expression in microarray experiments. Bioinformatics (Oxford, England). 2005;21:2067-2075. doi: 10.1093/bioinformatics/bti270

92. Ashburner M, Ball CA, Blake JA, Botstein D, Butler H, Cherry JM, Davis AP, Dolinski K, Dwight SS, Eppig JT, et al. Gene ontology: tool for the unification of biology. The Gene Ontology Consortium. Nat Genet. 2000;25:25-29. doi: 10.1038/75556

93. Zhou Y, Zhou B, Pache L, Chang M, Khodabakhshi AH, Tanaseichuk O, Benner C, Chanda SK. Metascape provides a biologist-oriented resource for the analysis of systems-level datasets. Nat Commun. 2019;10:1523. doi: 10.1038/s41467-019-09234 6

94. Shannon P, Markiel A, Ozier O, Baliga NS, Wang JT, Ramage D, Amin N, Schwikowski B, Ideker T. Cytoscape: a software environment for integrated models of biomolecular interaction networks. Genome Res. 2003;13:2498-2504. doi: 10.1101/gr.1239303

95. Piola M, Prandi F, Fiore GB, Agrifoglio M, Polvani G, Pesce M, Soncini M. Human Saphenous Vein Response to Trans-wall Oxygen Gradients in a Novel Ex Vivo Conditioning Platform. Ann Biomed Eng. 2016;44:1449-1461. doi: 10.1007/s10439 015-1434-0

96. Krom YD, Pires NM, Jukema JW, de Vries MR, Frants RR, Havekes LM, van Dijk KW, Quax PH. Inhibition of neointima formation by local delivery of estrogen receptor alpha and beta specific agonists. Cardiovasc Res. 2007;73:217-226. doi: 10.1016/j.cardiores.2006.10.024

SUPPLEMENTAL MATERIALS AND METHODS

SVPs isolation and mechanical stimulation

Saphenous Veins (SVs) of patients subjected to unilateral saphenectomy were collected for cell isolation (Table S1). Isolation of SVPs was performed according to the procedures described originally by Campagnolo et al[1]. In brief, the vein was mechanically minced and digested for 4 hours at 37°C with Liberase 2 (3,7 mg/mL, Roche). 70 µm and 40 µm cell strainer were used to remove the remaining aggregates. CD34+/CD31- cells were isolated by magnetic bead-assisted cell sorting (MACS, Miltenyi Biotec). SVPs were grown in a humidified atmosphere (95% air, 5% CO2) at 37°C using Endothelial Growth medium (EGM-2) supplemented with 2% Fetal Bovine Serum (FBS) and 1% Penicillin/Streptomycin (P/S, all by Lonza). The antigenic phenotype of expanded SVPs was described previously[2]. After expansion for 3 passages, CD31-/CD34+ were subjected to cyclic strain using the FlexCell Tension Plus FX-5000T system. Before cell seeding, six-well Bioflex plates were treated with sulfosuccinimidyl 6-(4'-azido-2'- nitrophenylamino) hexanoate (Sulfo-SANPAH) at 200 µg/ml in Hepes 50 mM (pH 8.5), photo-activated by exposure to UV-light (365 nm) and coated with fibronectin from human plasma (10µg/ml, Sigma-Aldrich). Cells at 105/well density were subjected to uniaxial cyclic deformation protocol (0-10% deformation, 1 Hz frequency) for 72 hours, while static controls were provided by seeding an equal number of cells, under the same atmospheric conditions, but without mechanical stimulation (see also a previous publication from our group[3]).

RNA extraction and RNA sequencing

After mechanical stimulation, RNA was extracted using TRIzol (Invitrogen), quantified with NanoDrop- 1000 spectrophotometer. Superscript III (Thermo Fisher Scientific) was used for reverse transcription. Quantitative real-time PCR analyses were performed with Power SYBR Green PCR Master Mix (Applied Biosystems) in an ABI 7900 Fast thermal cycler to detect gene amplification products (listed in Table S2). Expression levels were calculated relative to GAPDH mRNA, used as an internal standard control. Statistical analysis was done on the C_T values. The RNA sequencing methods have been already described in another a previous reference[3]. In brief, total RNA concentration and quality were assessed by microfluidics electrophoresis using the RNA 6000 Nano Assay Kit on the 2100 Bioanalyzer system (Agilent Technologies, Santa Clara, CA, United States). Samples with average RNA Integrity Number (RIN) value of 9.6 were considered for the analysis. RNA sequencing was performed and paired-end sequencing was chosen (Read1:R1, Read2:R2), where short reads (101 base pair in length) are obtained from ends of DNA fragments for high-throughput sequencing. Prior to further analysis, a quality check using FASTQC bioinformatics tool was performed on sequencing data.

Bioinformatics

The raw data on which the bioinformatic analyses are based are freely accessible at the European Nucleaotide Archive (Project: PRJNA792820; https://www.ebi.ac.uk/ena/browser/view/PRJNA792820). Sequential aligning of raw reads was performed against the GRCh38 Human Genome reference (version 99) with "STAR" [4], and "Bowtie 2" [5] to locally align any reads not mapped by STAR. Gene expression quantification and annotation was computed by "featureCounts" [6]. Raw counts were then imported into the R software v4.2.0. and pre-processed using the DaMiRseq R/Bioconductor package [7]. A filtering step was applied to retain genes with at least 10 counts in 50% of samples, while variance-stabilising transformation was used for data normalisation. Differential expression analysis (paired comparison) was performed using the limma R/Bioconductor package [8] and genes with an adjusted P - value < 0.05 (corrected by the Benjamini-Hochberg method) and an absolute log2 fold-change (FC) > 1 were considered as differentially expressed (DE). Unsupervised hierarchical clustering analysis was performed on the expression values of DE genes or genes of interest (e.g. Hippo pathway), based on the Euclidean and 1-pearson correlation metrics, for samples and genes, respectively, and the complete linkage method, as implemented in the GENE-E software v3.0.213. For functional inference analysis, we took advantage of prior knowledge of genes grouped according to the Gene Ontology gene-set collection [9] performed enrichment analysis using the Metascape software [10]. The up- and down-regulated DE genes as found by comparing "ON" vs. "OFF" condition were used as input gene lists, while the genes expressed in the present RNA-seq dataset were set as background.

To identify regulatory elements and infer transcription factors (TFs), we relied on a reverse engineering approach through cis-regulatory sequence analysis. The analysis was performed in the Cytoscape environment v3.10.0 [11] using the iRegulon software v1.3 [11] with default parameters to find sequence motifs in the promoter or distal regions and the possible transcription factors of up-regulated DE genes found by comparing the "ON" vs. "OFF" condition. To find out experimentally based interactions between regulatory sequences and TFs, we relied on 3 databases of 1120 chromatin immunoprecipitation sequencing (ChIP-seq) signals along the genome (i.e., tracks). The resulting tracks were ranked according to method's statistics, i.e. the normalized enrichment score (NES) and area under the cumulative recovery curve (AUC), clustered based on track (T) similarity, and labelled with a progressive number indicating the number of different cluster tracks. DE genes under the putative control of TEAD4 were subjected to enrichment analysis through the Metascape software to infer specific functional associations.

Cell biology/analysis methods

For experiments involving the use of TGF-β1, TSP-1, Forskolin (an inhibitor of the RhoA-dependent stress fibers formation) and Verteporfin (an inhibitor of the YAP/TAZ interaction with TEADs[12]) cells were plated onto plastic dishes in the presence

or the absence of the factors and/or the drugs at a factors and/or the drugs at 10 ng/ml, 50 ng/ml, 100 μM and 10 μM concentration, respectively. After treatments, cells were harvested for migration assays, RNA or total protein extraction for RT-qPCR or immunoprecipitation/western blotting. Immunofluorescence with the indicated antibodies was performed after fixing cells treated with the factors and/or the inhibitors with paraformaldehyde. For fluorescence quantification, computer-based image analysis was performed using Image-J or a CARE. Further details about cell biology/analyses are present in the extended online methods.

For immunofluorescence of cell cultures, cells were fixed with 4% paraformaldehyde and then permeabilized for 1 hour with PBS containing 3% (w/v) BSA and 1% (v/v) Triton X-100. Incubation with primary antibodies anti- YAP (Santa Cruz, 500 ng/ml), anti- Vinculin (Invitrogen, 5 ng/ml) and anti- PCNA (Dako, 3,27 μg/ml) was performed overnight at 4°C. Cells were then incubated for 1 hour at room temperature with the appropriate secondary antibodies (Invitrogen, 4 μg/mL), Phalloidin-TRITC (Sigma-Aldrich, 32 μg/mL) and DAPI nuclear dye (Dako, 50 μg/mL). Digital images were obtained using an Apotome fluorescence microscope (Carl Zeiss). Cell morphological analyses were performed using ImageJ software (1.48v- software for Java, National Institutes of Health, USA), as previously described[2].

In situ Proximity Ligation assay (PLA) was performed on SVPs fixed with 4% paraformaldehyde. DuoLink PLA technology probes and reagents (Sigma-Aldrich) were used following manufacturer's protocol. Cells were permeabilized with PBS containing 3% (w/v) BSA and 1% (v/v) Triton X-100 for 1 hour and then blocked with the blocking solution for 1 hour at 37°C. Primary antibodies anti-YAP (Santa Cruz, 500 ng/ml) and anti-phospho-SMAD3 (Invitrogen, diluted as indicated) were incubated overnight at 4°C. After washes with specific buffer, cells were incubated with PLA probes (anti-mouse MINUS and anti-rabbit PLUS) for 1 hour at 37°C. Ligation and amplification step were performed at 37°C for 30 and 100 minutes, respectively. Finally, cover slips were washed with PBS and mounted with Duolink in situ mounting medium containing DAPI. Images were acquired using ApoTome fluorescence microscope (Carl Zeiss) and quantification of cells with positive PLA signal was performed with ImageJ software.

Migration assays were performed using Transwells (Corning) as described previously[2]. In brief, SVPs were mechanically stimulated for 72 hours and then seeded in the upper part of the insert in a 24 well PET Transwell (8 μm pore membrane) in EGM-2 without FBS. In the lower compartment, two conditions were assayed: EGM-2 without FBS and EGM-2 plus 10% FBS. After 24 hours, migrating cells were fixed with 4% paraformaldehyde for 10 minutes, permeabilized with methanol for 20 minutes and stained with 1% (w/v) Crystal Violet diluted in 2% (v/v) ethanol for 30 minutes. Images were acquired with Axiovert 200M (Zeiss). For Crystal Violet quantification, the staining was solubilized with 2% (v/v) SDS and optical density (550 nm) was measured using Infinite M200 PRO reader (Tecan).

For immunohistochemistry on tissue sections, after heat-induced epitope unmasking (citrate buffer, pH 6, 10 minutes) and quenching with hydrogen peroxide (0.6%, 20 minutes), nonspecific binding was blocked with PBS containing 3% (w/v) BSA for 45 minutes. Sections were then incubated overnight with primary antibody against YAP (Cell Signalling, diluted as indicated) and against Thrombospondin-1 (Invitrogen, 5 µg/ml), followed by incubation with secondary antibody (goat anti-rabbit IgG-HRP, Invitrogen, 4 µg/ml) for 1 hour. Reaction was developed with diaminobenzidine and nuclei were counterstained with hematoxylin. For immunofluorescence, after antigen retrievel (DAKO Blue, pH 9, 98 degrees, 20 minutes) and nonspecific binding blocking (1% PBSA containg 2% Normal Goat Serum (NGS)), slides were incubated with primary antibody for ACTA2 (1:150) and CD31 (1:400). The following day, slides were incubated with goat anti-rabbit Alexa Fluor 555 (1:800) and Hoechst (1:800, Sigma 34580) to stain nuclei. Slides were scanned using Panoramic Scann II (3D Histech) or Zeiss Axio Scan. Movat Pentachrome was performed according to previous work[13].

Protein methods

Western blotting analyses were performed following protocols already published (2, 4). In brief, SVPs were lysed in a buffer containing 10 mM Tris-Cl, pH 7.4, 150 mM NaCl, 5 mM EDTA, 1% (v/v) Triton X-100, 1% (w/v) sodium deoxycholate, 0.1% (w/v) sodium dodecyl sulfate and 1% (v/v) protease and phosphatase inhibitor mixture (Sigma-Aldrich). After sonication, cell lysates were centrifuged for 15 min at 14 000 g and supernatants were collected; Proteins were quantified by BCA protein assay kit (Pierce Chemical Co). Cell lysates (30 µg per lane) were diluted in Laemli sample buffer, heated at 95°C for 5 minutes, run onto 4-12% gradient SDS-polyacrylamide gel (Invitrogen), and transferred to nitrocellulose membrane. The blots were blocked with Tris Buffered-saline containing 5% (w/v) bovine serum albumin (Sigma-Aldrich) for 1 hour at room temperature. Primary antibodies were incubated overnight at 4°C with (listed in Table S3) was performed to examine individual protein expression. Membranes were finally incubated with appropriate secondary antibodies for 20 minutes. Images were taken by LI-COR Odyssey and band densities were quantified using ImageJ software.

For immunoprecipitation, 100 µg of cell lysates were incubated overnight at 4°C with antibody against YAP (Santa Cruz, 2 µg) and protein G- agarose beads (Cell Signaling). The beads were then washed three times with the lysis buffer, and the immune complex was eluted in Laemli sample buffer. Lysates and immunoprecipitates were subjected to SDS-PAGE electrophoresis, followed by immunoblotting. Proteins were visualized using western blot chemiluminescence reagent (antibodies listed in Table S3).

Soluble collagen release was quantified using Sircol colorimetric assay (Biocolor) on conditioned medium of SVPs treated with TSP1/TGF-β ± VTP, following manufacturer's instructions. The colorimetric reaction was read at absorbance of 555 nm reading using Tecan Infinite M200 PRO spectrophotometer.

Ex vivo SV stimulation and in vivo arterialization models

The ex vivo stimulation of human-derived SVs graft was performed using a bioreactor that was conceived to create a continuous coronary-like counter-pulsed flow in 5 cm SV segments, as described by us previously[14]. To obtain samples to be used as controls, another bioreactor creating a steady flow pattern was employed[15]. A coronary flow/pressure condition (CABG) was obtained consisting of a counter-phased sinus-like flow rate at ~150 ml min-1 with a luminal pressure 80 - 120 mmHg and a 1 Hz pulse frequency. A control, venous perfusion (VP), flow was realized consisting of a constant flow rate at 5 ml min-1 and a 5-mmHg pressure.

After stimulation with the two platforms for 14 days, the vessels were unmounted from the platforms and processed for histology and histochemistry.

Arteriovenous bypass procedures in pigs were performed in female Landrace or Large White/Landrace crossbred pigs weighing 20 to 30 kg. A single dose of intramuscular ketamine into the neck (0.1 mg/Kg ketamine: Ketaset Injection Fort Dodge Animal Health Ltd, Southampton, UK) was performed as anesthesia and after endotracheal intubation, it was maintained using 2-3% halothane and oxygen. Animals ventilated spontaneously throughout. Pigs were euthanized with 100 mg/Kg intracardiac injection of pentobarbitone in a single dose (Euthatal; 200 mg/mL pentobarbital sodium, J.M. Loveridge Plc, Southampton, UK).

For vein graft disease model in mice, ApoE3*Leiden mice (bred in our own colony), 10-16 weeks old, were fed a diet containing 1% cholesterol and 0.5% cholate (Bio-Services B.V., Schaijk, Netherlands) to induce hypercholesterolemia for three weeks prior to surgery until sacrifice. Thereafter, male mice underwent vein graft surgery, in which a donor caval vein from either a female or male donor was inserted into the arterial circulation at the site of the right common carotid artery, as previously described. Mice were anesthetized intraperitoneally with 5 mg/kg of midazolam (Roche Diagnostics), 0.5 mg/kg of dexmedetomidine (Orion Corporation) and 0.05 mg/kg of fentanyl (Janssen Pharmaceutical). After surgery, the anaesthesia was antagonized with 2.5 mg/kg of atipamezol (Orion Corporation) and 0.5 mg/kg of flumazenil (0.5 mg/kg, Fresenius Kabi). An amount of 0.1 mg/kg of buprenorphine (MSD Animal Health) was given for pain relieve. Animals were sacrificed 28 days after the surgery, via exsanguination after anaesthesia (described above) followed by 3 min of in vivo perfusion-fixation with PBS and 4% formaldehyde (100496, Sigma- Aldrich, Saint Louis, USA). The vein grafts were harvested and fixed in 4% formaldehyde. All animals received food and water ad libitum. Mice were randomized based on age, body weight and plasma cholesterol levels (10017, Human Diagnostics, Wiesbaden, Germany).

Statistical analyses

The statistical analyses supporting the bioinformatics analysis of the RNAseq data are reported in the specific section of the extended online methods. The type of statistical tests to compare data presented in the bar graphs throughout

the study are specified in figure legends. Each bar has superimposed the number of experimental replicates, and a $P < 0.05$ was considered a significant value in statistical comparisons. Data were analyzed and graphically represented using the GraphPad software.

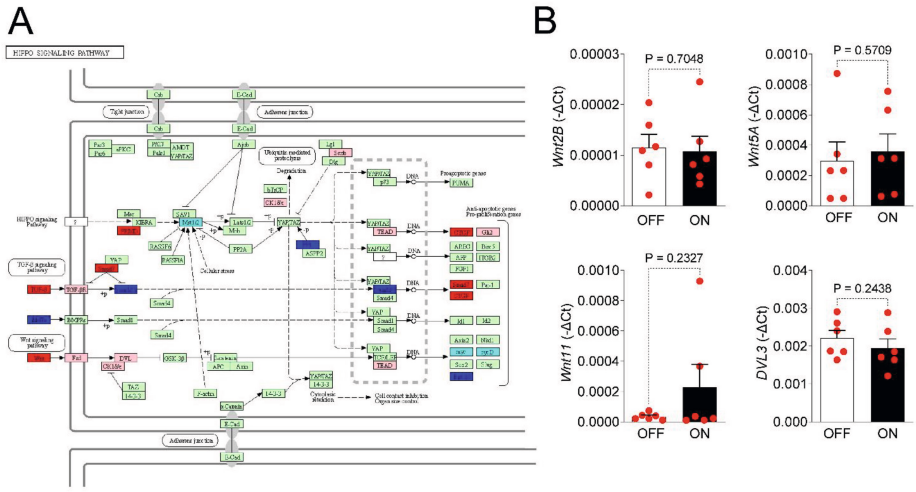

Figure S1.

(**A**) Kyoto Encyclopedia of Genes and Genomes (KEGG) map representation of the Hippo pathway with indication of the genes significantly upregulated (red/rose color) or downregulated (blue/light blue) by mechanical stimulation. (**B**) Involvement of Wnt signaling in mechanical-dependent phenotypic transformation was not confirmed by validation of the RNAseq data by RT-qPCR amplification of *Wnt2B*, *Wnt5A*, *Wnt11* and *DVL3* transcripts performed on independent RNA samples. In all graphs, red dots overlapped to the bars indicate the result of each experiment performed in independent cell lines. The P values resulting from pairwise t-test are indicated above the significance lines.

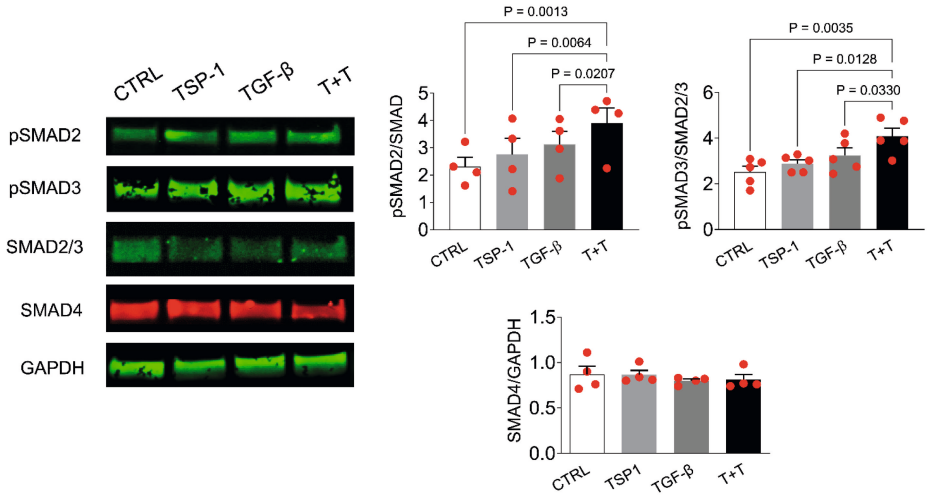

Figure S2.

Representative western analysis of proteins extracted from SVPs treated with TGF-β, TSP-1 and the T+T combination. Densitometric analysis of pSMAD2/SMAD2/3 and pSMAD3/ SMAD2/3 band intensities revealed that SVPs treated with the T+T combination had a higher level of pSMAD2 and pSMAD3 phosphorylation, indicative of a higher transcriptional activity. In all graphs, red dots overlapped to the bars indicate the result of each experiment performed in independent cell lines. The P values resulting from 1-way ANOVA (repeated measures) with Tukey post-hoc are indicated above the significance lines.

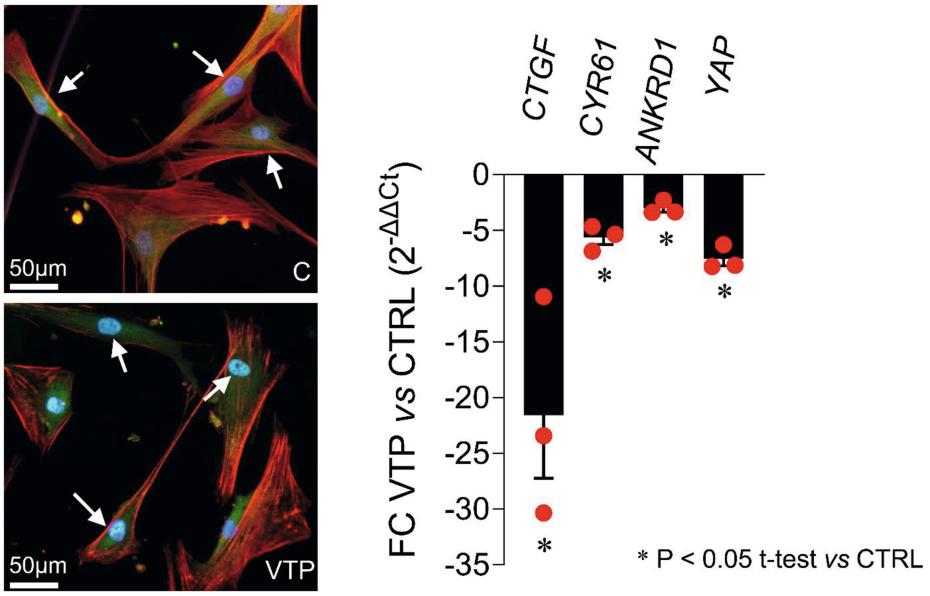

Figure S3.

Treatment with Verteporfin (VTP) has no effect on YAP nuclear localization (compare the upper and the lower panel) but has a strong inhibition effect on YAP target genes *CTGF*, *CYR61* and *CTGF*, and YAP expression itself, as determined by RT-qPCR. The graph on the right represents the negative fold changes in expression of the indicated genes compared to the controls. In the graph, the red dots overlapped to the bars indicate the result of each experiment performed in independent cell lines. mRNA expression data were compared by 1-way ANOVA (repeated measures) with Tukey post-hoc. Asterisks indicate a $P < 0.05$ in the treatment vs. control comparison.

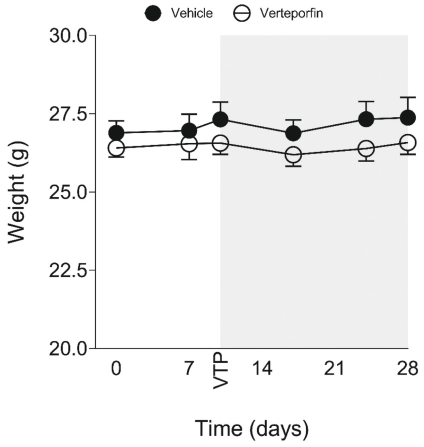

Figure S4.

VTP treatment does not affect the animal well-being as assessed by periodic assessment of body weight, before (left) and after (right) VTP injection.

Table S1. Clinical and demographical characteristics of patients underwent (saphenectomy). Data are presented as percentages or mean ± SD.

Variable	Saphenectomy patients (n = 44)
Age (y)	55 ± 13
Male, n (%)	23 (52%)
Hypertension, n (%)	2 (4.5%)
Dyslipidaemia, n (%)	6 (13.6%)
Diabetes, n (%)	10 (22.7%)
Body mass index	27 ± 4
Smoking, n (%)	22 (50%)
Glycaemia	106 ± 17
Creatinine	0.8 ± 0.2

Table S2. Sequence of oligonucleotides employed for RT-qPCR analysis

GENE	SEQUENCE
hCTGF	Forward: 5'-AGGAGTGGGTGTGTGACGA-3' Reverse: 5'-CCAGGCAGTTGGCTCTAATC-3'
hCYR61	Forward: 5'-CCTTGTGGACAGCCAGTGTA-3' Reverse: 5'-ACTTGGGCCGGTATTTCTTC-3'
hANKRD1	Forward: 5'-AGTAGAGGAACTGGTCACTGG-3' Reverse: 5'-TGGGCTAGAAGTGTCTTCAGAT-3'
hYAP	Forward: 5'-CACCTGTATCCATCTCATCCAC-3' Reverse: 5'-ACGACCAATAGCTCAGATCCT-3'
hCOL1A	Forward: 5'-GGACACAGAGGTTTCAGTGG-3' Reverse: 5'-CCAGTAGCACCATCATTTCC-3'
hFZD8	Forward: 5'-TTTCTCCCTCGACTCTTCCTA-3' Reverse: 5'-GAATACCCAAACCGTGCAATC-3'
hTGF-ß1	Forward: 5'-CCGACTACTACGCCAAGGA -3' Reverse: 5'-GTTCAGGTACCGCTTCTCG-3'
hSMAD3	Forward: 5'-ACGACTACAGCCATTCCATC-3' Reverse: 5'-CTCCATCTTCACTCAGGTAGC-3'
hSMAD7	Forward: 5'-CGCACCTTTGGAGTTTTGG-3' Reverse: 5'-CACAGCATCTGGACAGTCTG-3'
hWNT-2b	Forward: 5'-ATACCTACACAGTCAGCGTTC-3' Reverse: 5'-GGATATTGTCACAGATCACTCGT-3'
hWNT-5a	Forward: 5'-TGCCAGTATCAATTCCGACATC-3' Reverse: 5'-GCTCACCGCGTATGTGAAG-3'
hWNT-11	Forward: 5'-GCCAATAAACTGATGCGTCTAC-3' Reverse: 5'-CACTTACACTTCATTTCCAGAGAG-3'
hDVL3	Forward: 5'-TCATCCGCCATACCGTCA-3' Reverse: 5'-GATCGTGGAGAGACAGGTTG-3'
hTAGLN	Forward: 5'-ACAAACTCATCTTCCTCAAGCC-3' Reverse: 5'-CTTCTCATTTTCCATTCCCTTCAC -3'
hACTA2	Forward: 5'-AGAGTTACGAGTTGCCTGATG-3' Reverse: 5'-CTGTTGTAGGTGGTTTCATGGA-3'
hTHBS1	Forward: 5'-TGAGGAGGACACTGGTAGAG -3' Reverse: 5'-GGGCCTCAATGACAATTTCC -3'
hCD47	Forward: 5'-GGAGGTTGTATAGTCTTCTGATTGG -3' Reverse: 5'-TTGGACTGAGTCTCTGTATTGC -3'
hGAPDH	Forward: 5'-AATCCCATCACCATCTTCCAG-3' Reverse: 5'-AAATGAGCCCCAGCCTTC-3'

Table S3. List of the antibodies employed in the present study.

ANTIBODY	HOST	MANUFACTURER	CONCENTRATION
YAP	Mouse	Santa-Cruz	100 ng/mL
αSMA	Mouse	Santa-Cruz	Diluted as indicated
CD31	Rabbit	AbCam	Diluted as indicated
Phospho-YAP	Rabbit	Cell Signaling	Diluted as indicated
LATS	Goat	Santa-Cruz	200 ng/mL
Phospho-LATS	Rabbit	Cell Signaling	Diluted as indicated
Phospho-SMAD2	Rabbit	Cell Signaling	Diluted as indicated
Phospho-SMAD3	Rabbit	Invitrogen	Diluted as indicated
SMAD2/3	Mouse	BD Biosciences	250 ng/mL
SMAD4	Rabbit	Cell Signaling	Diluted as indicated
Pan TEAD 1-4	Rabbit	Cell Signaling	Diluted as indicated
Pan 14-3-3	Rabbit	Cell Signaling	Diluted as indicated
SM22-α	Rabbit	Abcam	1 µg/mL
GAPDH	Mouse	Santa-Cruz	100 ng/mL
CD31	Rabbit	Abcam	125 ng/mL
ACTA2	Mouse	Santa-Cruz	1 µg/mL
Hoechst	-	Sigma	25 µM
555 anti-rabbit	Goat	Invitrogen	1.25 µg/mL
680 anti-rabbit	Donkey	LI-COR	100 ng/mL
800 anti-mouse	Donkey	LI-COR	100 ng/mL
800 anti-rabbit	Donkey	LI-COR	100 ng/mL
Anti-rabbit IgG-HRP	Goat	Invitrogen	160 ng/mL
Anti-mouse IgG-HRP	Rabbit	Invitrogen	160 ng/mL

SUPPLEMENTAL MATERIAL REFERENCES

1. Campagnolo P, Cesselli D, Al Haj Zen A, Beltrami AP, Kränkel N, Katare R, Angelini G, Emanueli C, Madeddu P. Human adult vena saphena contains perivascular progenitor cells endowed with clonogenic and proangiogenic potential. *Circulation*. 2010;121:1735-1745. doi: 10.1161/circulationaha.109.899252
2. Garoffolo G, Ruiter MS, Piola M, Brioschi M, Thomas AC, Agrifoglio M, Polvani G, Coppadoro L, Zoli S, Saccu C, et al. Coronary artery mechanics induces human saphenous vein remodelling via recruitment of adventitial myofibroblast-like cells mediated by Thrombospondin-1. *Theranostics*. 2020;10:2597-2611. doi: 10.7150/thno.40595
3. Maselli D, Garoffolo G, Cassanmagnago GA, Vono R, Ruiter MS, Thomas AC, Madeddu P, Pesce M, Spinetti G. Mechanical Strain Induces Transcriptomic Reprogramming of Saphenous Vein Progenitors. *Front Cardiovasc Med*. 2022;9:884031. doi: 10.3389/fcvm.2022.884031
4. Dobin A, Davis CA, Schlesinger F, Drenkow J, Zaleski C, Jha S, Batut P, Chaisson M, Gingeras TR. STAR: ultrafast universal RNA-seq aligner. *Bioinformatics (Oxford, England)*. 2013;29:15-21. doi: 10.1093/bioinformatics/bts635
5. Langmead B, Salzberg SL. Fast gapped-read alignment with Bowtie 2. *Nature methods*. 2012;9:357- 359. doi: 10.1038/nmeth.1923
6. Liao Y, Smyth GK, Shi W. featureCounts: an efficient general purpose program for assigning sequence reads to genomic features. *Bioinformatics (Oxford, England)*. 2014;30:923-930. doi: 10.1093/bioinformatics/btt656
7. Chiesa M, Colombo GI, Piacentini L. DaMiRseq-an R/Bioconductor package for data mining of RNA- Seq data: normalization, feature selection and classification. *Bioinformatics (Oxford, England)*. 2018;34:1416-1418. doi: 10.1093/bioinformatics/btx795
8. Smyth GK, Michaud J, Scott HS. Use of within-array replicate spots for assessing differential expression in microarray experiments. *Bioinformatics (Oxford, England)*. 2005;21:2067-2075. doi: 10.1093/bioinformatics/bti270
9. Ashburner M, Ball CA, Blake JA, Botstein D, Butler H, Cherry JM, Davis AP, Dolinski K, Dwight SS, Eppig JT, et al. Gene ontology: tool for the unification of biology. The Gene Ontology Consortium. *Nat Genet*. 2000;25:25-29. doi: 10.1038/75556
10. Zhou Y, Zhou B, Pache L, Chang M, Khodabakhshi AH, Tanaseichuk O, Benner C, Chanda SK. Metascape provides a biologist-oriented resource for the analysis of systems-level datasets. *Nat Commun*. 2019;10:1523. doi: 10.1038/s41467-019-09234-6
11. Shannon P, Markiel A, Ozier O, Baliga NS, Wang JT, Ramage D, Amin N, Schwikowski B, Ideker T. Cytoscape: a software environment for integrated models of biomolecular interaction networks. *Genome Res*. 2003;13:2498-2504. doi: 10.1101/gr.1239303
12. Garoffolo G, Casaburo M, Amadeo F, Salvi M, Bernava G, Piacentini L, Chimenti I, Zaccagnini G, Milcovich G, Zuccolo E, et al. Reduction of Cardiac Fibrosis by Interference With YAP-Dependent Transactivation. *Circ Res*. 2022;131:239-257. doi: 10.1161/CIRCRESAHA.121.319373
13. de Jong A, Sier VQ, Peters HAB, Schilder NKM, Jukema JW, Goumans M, Quax PHA, de Vries MR. Interfering in the ALK1 Pathway Results in Macrophage-Driven Outward Remodeling of Murine Vein Grafts. *Front Cardiovasc Med*. 2021;8:784980. doi: 10.3389/fcvm.2021.784980
14. Piola M, Ruiter M, Vismara R, Mastrullo V, Agrifoglio M, Zanobini M, Pesce M, Soncini M, Fiore GB. Full Mimicking of Coronary Hemodynamics for Ex-Vivo Stimulation of Human Saphenous Veins. *Ann Biomed Eng*. 2017;45:884-897. doi: 10.1007/s10439-016-1747-7
15. Piola M, Prandi F, Fiore GB, Agrifoglio M, Polvani G, Pesce M, Soncini M. Human Saphenous Vein Response to Trans-wall Oxygen Gradients in a Novel Ex Vivo Conditioning Platform. *Ann Biomed Eng*. 2016;44:1449-1461. doi: 10.1007/s10439-015-1434-0